Załącznik nr 3

Self-presentation

1. Name and last name: Michał Janusz Pawlak

2. Held diplomas and scientific degrees, place and year of their acquisition and the title of the doctoral thesis:

January 2011 – July 2014
Technical University of Koszalin, **doctor degree in technical science : electronics**; title of thesis: *Thermal and plasma waves in semiconductors*, supervisor: prof. dr. hab. Mirosław Maliński

October 2005 – January 2012
Warsaw University of Technology, Faculty of Electronics and Information Technology, degree course: electronics and telecommunication, specialty: multimedia technology, title: **engineer**

April 2004 – March 2007
Ruhr Uniwersity Bochum, Germany, Faculty of Physics and Astronomy, Doctoral Study, degree: Doctor of physical sciences **(doktor rer. nat.),** thesis title: Thermal and electrical properties of semiconductors measured by means of photopyroelectric and photocarrier radiometry techniques, supervisor: prof. dr Josef Pelzl
A defense of doctoral thesis 01.2010.

October 1991 – June 2001
Nicolaus Copernicus University, Faculty of Physics, Astronomy and Informatics, degree course: physics, specialty optoelectronics and laser physics; title: **Master of science**;

October 1996 – June 1999 assistant
Nicolaus Copernicus University, Faculty of Physics, Astronomy and Informatics, degree course: physics, specialty experimental physics; title: **Bachelor of science**;

3. Information on employment in scientific institutions:

04.2007 –08.2007 Assistent at Ruhr University Bochum, Germany
09.2007 – 04.2008 Assistent at University of Toronto, Canada
11.2008 – 03.2009 Asystent at Ruhr University Bochum, Germany
03.2012 – now – Adjunct at Institution of Physics NCU

4. Achievement indicated in accordance with the Art. 16 Item 2 of the Act of 14 March 2003 on Academic Degrees and Title and Degrees and Title in Art (Journal of Laws No. 65, item. 95 with later amendments):

As a scientific achievement resulting from the act, I point monothematic series of publications under the collective title:

New infrared methods for investigation of the semiconductor materials.

H1. M. Pawlak, M. Chirtoc, N. Horny, J. Pelzl, Spectrally Resolved Modulated Infrared Radiometry (SR-MIRR) of Photothermal, Photocarrier and Photoluminescence Response of CdSe Crystals: Determination of Optical, Thermal and Electronic Transport Parameters, J. Appl. Phys. 119 (2016); 125108, IF = 2.068;

H2. M. Pawlak, K. Strzałkowski, Identification of the photoluminescence response in the frequency domain modulated infrared radiometry signal of ZnTe:Cr bulk crystal, Infrared Phys. Techn. 78 (2016); 190 – 194, IF = 1.713

H2a M. Pawlak, Comments on the paper: M. Pawlak, K. Strzałkowski, Identification of the photoluminescence response in the frequency domain modulated infrared radiometry signal of ZnTe:Cr bulk crystal, Infrared Phys. Techn. 78 (2016) 190–194, Infrared Phys. Techn. 85 (2017); 502 – 503, IF = 1.851

H3. M. Pawlak, M. Streza, C. Morari, K. Strzałkowski, M. Depriester, M. Chirtoc, Quantitative Thermal Wave Phase Imaging of an IR semi-transparent GaAs wafer using IR lock-in thermography, Meas. Sci. Technol. 28 (2017); 025008, IF = 1.685

H4. M. Pawlak, A. Panas, A. Ludwig, A.D. Wieck, On measurement of the thermal diffusivity of moderate and heavily doped semiconductor samples using modulated photothermal infrared radiometry, Thermochim. Acta 650 (2017); 33 – 38, IF = 2.189

H5. M. Pawlak, S. Pal, A. Ludwig, A.D. Wieck, On the infrared absorption coefficient measurement of thick heavily Zn doped GaAs using spectrally resolved modulated photothermal infrared radiometry, J. Appl. Phys. 122 (2017); 135109 , IF = 2.176

H6. M. Pawlak, S. Pal, S. Scholz, A. Ludwig, A.D. Wieck, Simultaneous measurement of thermal conductivity and diffusivity of an undoped Al0.33Ga0.67As thin film epitaxially grown on a heavily Zn doped GaAs using spectrally-resolved modulated photothermal infrared radiometry, Thermochim. Acta 662 (2018) 59-64, IF = 2.189

H7. M. Pawlak, On radiative lifetime measurement of chromium transitions in Cr doped ZnSe and ZnTe crystals using the frequency domain modulated infrared radiometry, Infrared Phys. Techn. 92 (2018) 90-95, IF= 1.851,

H8. M. Pawlak, N. Horny, S.Scholz, C. Ebler, A. Ludwig, A.D. Wieck, Simultaneous measurement of infrared absorption coefficient of a C doped Al0.33Ga0.67As thin film and thermal boundary resistance between the thin film and heavily Zn doped GaAs substrate using spectrally-resolved modulated photothermal infrared radiometry, Thermochim. Acta 667 (2018) 73-78, IF = 2.189

H9. M. Pawlak, Simple method for determination the effective infrared absorption coefficient of semiconductor wafer using the modulated photothermal infrared radiometry, Infrared Phys. Techn. 97 (2019) 43-47, IF= 1.851

1. Introduction

Spectroscopic methods are important experimental tools to investigate micro- and macroscopic properties of semiconductors. Among the optical spectroscopic methods which are based on the interaction of light with matter the modulated photothermal infrared radiometry (PTR) that was for a first time applied by Nordal and Kanstada in 1979 [1], has attracted much attention in recent years. PTR is a non-contact method which allows to measure simultaneously thermal and electronic properties of a semiconductor material. An intensity modulated light beam is used to excite locally thermal waves and plasma waves in the sample. The response (PTR signal) is an amplitude modulated infrared (IR) emission that usually is detected by an IR-sensor covering the IR wavelength range between 2 μm and 12 μm. PTR experiments can also be performed in the time domain using pulsed excitation. In the case of small signal output frequency domain measurements are mostly of advantage as the lock-in technique can be applied. In addition, measurements of the IR-response as a function of the modulation frequency offer the unique possibility to retrieve the depth dependence of the thermal and electronic properties of the sample. Initially the PTR method was mainly used for the investigation of infrared opaque materials. Infrared semi-transparent and transparent samples are frequently covered by a thin IR opaque layer before the measurements were performed. The latter procedure, however, has the disadvantage that the supplemental layer complicates the analysis as additional parameters such as the thermal properties of the layer and thermal boundary resistance between the layer and the sample have to be taken into consideration [2,3].Therefore, other concepts have been developed that take into account the infrared properties for the interpretation of the PTR signals from IR semi-transparent samples. In paper [4], the PTR method was used to investigate an infrared semi-transparent sample: a 48 μm-thick layer of grey paint layer on brass. Assuming an effective finite infrared absorption coefficient which is constant across the thin layer and independent of the wavelength in the detector bandgap the authors could well explain the observed dependence of the signal phase as a function of the modulation frequency. By numerical simulations Majaron et al. [5] demonstrated that the use of a constant effective IR absorption coefficient could lead to large errors in the PTR temperature depth profiles if the IR absorption coefficient varies markedly with the wavelength. This negative effect has been partially prevented by the authors in Ref. [6] and [7] who investigated a 5 μm thin SiC layer on silicon and silicon nitride on a quartz substrate by placing two different IR band pass filters in front of the detector.

One of the achievements of the above series of publications was to develop models to estimate infrared, electronic and thermal parameters of non-IR opaque one layer [H1, H3, H4, H5] and two layers samples [H6, H8]. It was found that in order to retrieve reliable information about thermal and electronic properties of the sample the knowledge of the infrared properties is essential. A possible way to determine the infrared properties could be supplementary FTIR measurements. However, in most cases, these additional experiments

would require different shape and preparation of the sample. An alternative approach developed in this series of publications is based on a spectral resolved PTR (SR-PTR) experiment that measures IR optical properties in defined wavelength gaps simultaneously with thermal and electronic parameters. This procedure offers the unique ability to measure the IR absorption coefficient together with the other properties at the same location, avoiding errors due to different spatial variation of the quantities. Compared to the previous works [6, 7] the spectral resolution of the SR-PTR method could be considerably improved. The estimated values of the infrared absorption coefficient obtained by SR-PTR are in good agreement with the values determined by the FTIR method where the latter technique could be applied. It could be shown that the SR-PTR method is very suited for the investigation of thick highly IR absorbing samples where FTIR fails. So it was possible with the SR-PTR method to measure the infrared absorption coefficient of a thick heavily Zn doped GaAs wafer [H5] where the FTIR method in the transmission configuration could not be applied and the FTIR method in the reflection configuration deliverd unreliable data. Furthermore, when a thin film was deposited on the sample also the infrared absorption coefficient of the thin film could be determined with the SR-PTR method whereas supplementary FTIR measurements (in reflection configuration) conducted on an undoped AlGaAs thin film provided only information on the layer thickness [H6]. With the PTR method it is also possible in addition to measure the thermal resistance interface between the thin layer and substrate. So it was found that the thermal boundary resistance between C-doped AlGaAs thin layer and GaAs substrate is two order of magnitude larger than that between undoped AlGaAs thin layer and GaAs substrate. This effect was attributed to the modulation doping of the thin layer. Thus, the simultaneous measurement of the thermal boundary resistance and the infrared absorption coefficient (which is proportional to the doping concentration) offer an unique possibility to study this effect more deeply. The infrared absorption coefficient is (usually) proportional to the doping concentration. It is worth mentioning that characterization of the thin film deposited on the heavily doped substrate using electrical methods is not trivial. For C-doped AlGaAs thin film a direct determination of this doping concentration by an electrical method was not possible due to the following reasons: The high doping lead to severe leakage of Au-Schottky gates and thus capacitance-voltage spectroscopy was impossible. In addition, it was not possible to discriminate the Hall parameters of the thin film from those of the heavily Zn doped substrate. For an undoped AlGaAs the use of Hall measurement alone are not sufficient. With the help of the PTR method all these problems could be largely overcome.

In the case of semiconducting materials, additional information about electronic transport (recombination) properties such as carrier recombination lifetime τ, carrier diffusivity D and surface recombination velocities S_1 and S_2 can be obtained by the investigation of the change of the IR emittance caused by the plasma waves Δn (plasma wave response) [8-11]

$$S_{PTR} \sim S_{termiczny}(\beta_{IR}, \alpha, k, L) + S_{plazmowy}(\tau, D, S_1, L), \quad (1)$$

Where β_{IR} is the infrared absorption coefficient, L is the sample thickness, α is the thermal diffusivity and k is the thermal conductivity. Moreover, the physical origin of the measured recombination lifetime can be retrieved from spectrally-resolved measurements and

appropriate IR filtered PTR signal. For the first time, it was also demonstrated that using the SR-PTR method possible photoluminescence contributions to the PTR signal can be separated from thermal- and plasma wave responses [H1, H2, H7].For this reason a different name the "modulated infrared radiometry" has been introduced.

PTR experiments are usually performed using a laser beam in the visible spectral range, which excites thermal and plasma waves at one point on the surface of the sample. To study the spatial variation of the thermal and infrared parameters lock-in thermography was applied using the thermal wave formalism which takes into account the infrared properties of the sample [H3]. The results of these published research works form a basis for the development of a new type of the infrared spectrometer which combines features of calorimetric and spectroscopic measurement devices. Due to similarities of the PTR method with a lock-in thermography all methods can be used to establish thermal and infrared images of the samples.

My recently published scientific work including the papers H1-H9 has been honored by an invitation for a Perspective article ((https://scitationinfo.org/p/1XPS-3F8/jappphys-invited-perspectives)) devoted to the topic "Photothermal and photocarrier phenomena in semiconductors" (see attached invitation letter). The article which is under preparation will be published in the Journal of Applied Physics, which is one of the most prestigious international journal in this field.

2. Theoretical background

For single-detector thermal wave methods, like modulated photothermal infrared radiometry, the measured signal is emitted only from a small area of the sample (when the beam size is much smaller than the sample area) or provide an average value of the investigated parameters (when the beam size is comparable with the sample area). The investigated surface of the sample is also limited by the detector area which is usually about 1x1 mm^2. Moreover, depending on the beam size diameter d of the exciting laser, the measured signal can depend both on in-plane and in-depth thermal properties (thermal diffusivity α and thermal conductivity k) of the sample (Fig 1 a and b), due to different dimensionality of heat propagation. Fig. 1a shows that one cannot neglect the lateral heat propagation in the case of three dimensional heat propagation and the signal is not only sensitive on in-depth thermal parameters but depends also on in-plane thermal parameters [12]. In contrast to single detector methods, the lock-in thermography method can provide the spatial information due to a larger active area and spatially separated quantum detectors. When the beam size covers a large area of the sample surface and the infrared radiation is measured on the other side (Fig 1c) one measures in-depth thermal properties of the sample. On the other hand, when the beam size is very small and the infrared radiation is measured on the same side, one can measure in-plane thermal properties of the sample (Fig. 1d) [13]. This modification of the experimental set-up provides a great advantage of lock-in infrared thermography over the conventional modulated photothermal infrared radiometry method in measuring in-plane/in-depth thermal properties of the samples.

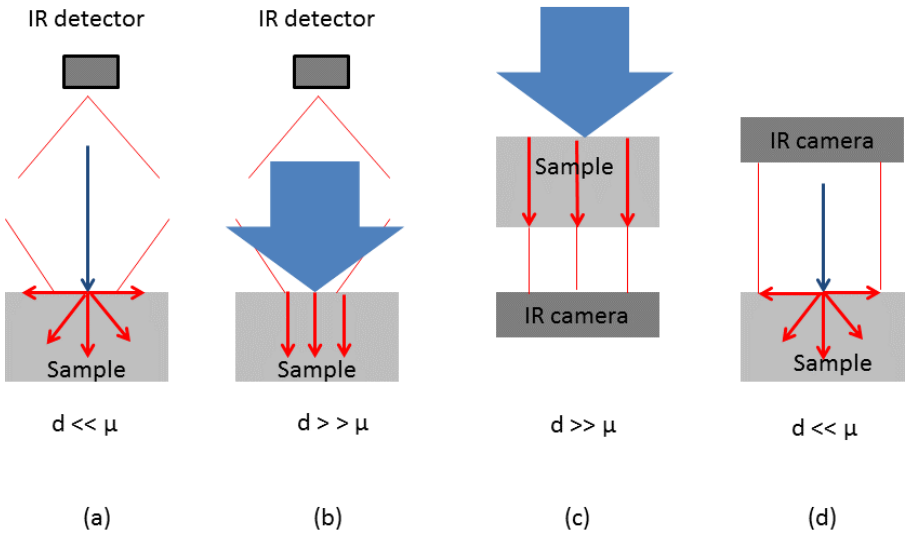

Figure 1. Comparison between measurements of in-plane (a,d) and in-depth thermal properties (b,c) of an IR opaque sample (the signal is emitted only from the surface of the sample), using modulated photothermal infrared radiometry and lock in thermography methods. Thermal diffusion length is defined as $\mu=sqrt(\alpha/(\pi f))$, where α is the thermal diffusivity of the sample and f is the modulation frequency of the excitation source and d is a laser beam diameter. Blue arrows - the excitation source. Red arrows - prevailing diffusion of the heat [13] and L is the sample thickness.

The PTR measurements are conducted in the reflection configuration on Fig. 1 a and b. When instead of IR camera is placed an IR detector then the measurements are conducted in the transmission configuration. It is worth mentioning that the reflection configuration is more suitable for investigation of the thin films.

For the one layer IR semi-transparent sample, $\beta_{IR} \cdot L << 1$, the PTR signal in the reflection configuration (Fig.1b) can be written as [3, H4, H5]

$$S(f,\beta_{IR}) \propto \int_0^L \beta_{IR} \cdot \Delta T(z,f) \cdot \exp(-\beta_{IR} \cdot z) dz\,, \tag{2}$$

where L is the sample thickness, β_{IR} is the infrared absorption coefficient, f is the modulation frequency, and

$$T(z,f) = \frac{I_0}{2k\sigma_t} \frac{1+R_{mb}e^{-2\sigma_t(L-z)}}{1-R_{mb}e^{-2\sigma_t L}} e^{-\sigma_t z}\,, \tag{3}$$

where $R_{ij}=(b_{ij}-1)/(b_{ij}+1)$,$b_{ij}=e_i/e_j$. e_i is the effusivity ($i=m$ refers to the material, $i = b$ refers to air), $\sigma_t(f)=sqrt(i \cdot 2 \cdot \pi \cdot f/\alpha)= (1+i)/\mu$ is the complex thermal wave vector, where α is the thermal diffusivity, k is the thermal conductivity, I_0 is the intensity of the incident radiation and $\mu=[\alpha/(\pi f)]^{1/2}$ is the thermal diffusion length.

Integrating expression (3) using formula (2) one obtains the following expression for the PTR signal [H4]

$$S_{PT}(f,\beta_{IR}) = \frac{I_0}{2k\left(\beta_{IR}^2 - \sigma_t^2\right)} \frac{(t-1) + (t+1)R_{mb}e^{-2\sigma_t L} + 2e^{-\beta_{IR}L}e^{-\sigma_t L}\left(\frac{b_{bm}-t}{b_{bm}+1}\right)}{1 - R_{mb}e^{-2\sigma_t L}}. \quad (4)$$

It is worth mentioning that the equivalent expression can be obtained from the expression for an optically opaque sample by simply exchanging the optical absorption coefficient with infrared one, due to symmetry of both absorption coefficients [14, 15, H1]

$$S_{PTR}(f,\beta_{IR}) = \frac{(1-i)T_{Ins}}{\sqrt{4\pi f}e} \frac{t}{t+1} \frac{1+M^{-2}(t+1)/(t-1)-2e^{-\beta_{IR}L}M^{-1}t/(t-1)}{1-M^{-2}} \quad (5)$$

The heat losses to ambient air are neglected. The instrumental constant T_{Ins} contains the power of the excitation radiation and establishes the proportionality between measured electrical signal and the temperature oscillations integrated over the sample thickness. The notations are: $t = \beta_{IR}/\sigma = (1/2)(1\text{-}i)\beta_{IR}\mu$ is the thermo-optical sample thickness, *e is* the thermal effusivity and $M = \exp(\sigma L) = \exp[(1+i)L/\mu)]$.

For high resistivity semiconductor samples, when $\beta_{IR} \cdot L << 1$, formula 2 can be simplified to the following formula [7-11]

$$S_{PTR}(f,\beta_{IR}) = a_{PT}(\beta_{IR})\int_0^L \Delta T(z,f)dz + b_{PC}\int_0^L \Delta n(z,f)dz. \quad (6)$$

The expressions for coefficients a_{PT} and b_{PC} as well as those for the thermal wave (temperature modulation) ΔT and the plasma wave (photoinjected free-carrier density) Δn in the case of Si photoconductive devices can be found in [8]. In this model, the infrared absorption coefficient is included in the coefficient a_{PT}, while b_{PC} is proportional to λ^2 (according to Drude theory). In fact, the temperature distribution presented in Ref. 9 is rather applies to semiconductors, because it takes into account the physical processes such as the thermalization, and diffusion of the carriers and subsequent recombination in the bulk or at the surface (surface recombination velocities). However, the signal simulations show very poor influence of thermalization and diffusion of the carriers [16] and the this model can be used exchanged with formulas (4) and (5) [17].

In case of integral measurements of the induced IR radiation, the absorption coefficient represents an effective value β_{eff} given by the following formula [18]:

$$\beta_{eff,IR} = \frac{\int_{\lambda_{\min}}^{\lambda_{\max}} R_{\det}(\lambda)\, W'_{\lambda}\, \beta_{IR}(\lambda)\, d\lambda}{\int_{\lambda_{\min}}^{\lambda_{\max}} R_{\det}(\lambda)\, W'_{\lambda}\, d\lambda}. \quad (7)$$

In this equation, $\beta_{IR}(\lambda)$ is the IR absorption coefficient spectrum of the sample and λ_{min} and λ_{max} are the sensitivity limits of the detector, $R_{det}(\lambda)$ is the spectral sensitivity of the detector, and $W'_{\lambda} = (\partial W/\partial T)_{\lambda}$ is the temperature derivative of Planck's expression for the spectral radiance.

The above discussed models assumed that the optical absorption takes place at the surface (the so called : surface heating models). In the paper [H5] the effect of the optical penetration depth ($1/\beta_{opt}$) on the PTR characteristics was investigated. It was found that the assumption of the surface heating in Eq. 2 is valid only for band-to-band excitation in semiconductor samples.

For the two-layer sample, the expression for the signal can be obtained similarly to the expression of one-layer sample (Eq.2) [H6, 19, H8]:

$$S(f) = \int_0^{L_1} \beta_{IR,1}\Delta T_1\left(f,z,\beta_{opt,1}\right)e^{-\beta_{IR,1}z}dz + \int_{L_1}^{L_2} \beta_{IR,2}\Delta T_2\left(f,z,\beta_{opt,2}\right)e^{-\beta_{IR,2}(z-L_1)}dz, \quad (8)$$

where f, $\beta_{opt,i}$, $\beta_{IR,i}$, L_i are the modulation frequency, the optical absorption coefficients in the visible and infrared spectral range, and the thickness of the thin film (with index i = 1) and substrate (with i = 2). The temperature distributions $\Delta T_1(f,z,\beta_{opt,1})$ and $\Delta T_2(f,z,\beta_{opt,2})$ are described by the following formulas [20]:

$$\Delta T_1\left(f,z,\beta_{opt,1}\right) = \Gamma e^{-\beta_{opt,1}z} + Ae^{-\sigma_1 z} + Be^{\sigma_1 z}, \quad (9)$$

$$\Delta T_2\left(f,z,\beta_{opt,2}\right) = \Sigma e^{-\beta_{opt,2}(z-L_1)} + Le^{-\sigma_2(z-L_1)} + Ge^{\sigma_2(z-L_1)}. \quad (10)$$

where $\sigma_i(f)$ is the complex thermal wave vector of the substrate (i=2) or thin layer (i=1). Expressions for the coefficients in eq. 8 and 9 can be found in Ref. 20.

As it was already mentioned, for high resistivity samples in the PTR signal the plasma wave component response can also appear. The plasma waves Δn are oscillating in time and space of the carrier concentration. For the semi-infinite and optically opaque (for the excitation source) sample, Sheard [21] gave a simplified expression for the integrated Δn:

$$\int_0^L \Delta n\left(z, f, \beta_{VIS}\right)dz = \frac{\eta I_0(1-e^{-\sigma_n L})}{h\nu\sigma_n\left(\sigma_n D_n + S_1\right)} \quad (11)$$

where $\sigma_n=[(1+i\omega\tau_c)/(D_n\tau_c)]^{1/2}$ is the complex wave number of the plasma wave, D_n is the carrier diffusion coefficient, S_1 is the surface recombination velocity at the front sample surface, τ_c is the bulk recombination lifetime of the photocarriers, η is the photocarrier generation efficiency and ν is optical frequency. In the case of a semiconductor with small values of D_n and $S_{1,2}$ (both sample surfaces are polished and etched), the formula (10) can be further simplified and the PC component in formula (10) reduces to [H1]:

$$S_{PC}(f,\lambda) = \frac{C\lambda^2\eta\tau_c}{1+i\omega\tau_c}. \quad (12)$$

The constant C contains instrumental factors and other sample parameters occurring in the coefficient b_{PC}. Formula (12) contains the factor λ^2 which originates from the Drude model relating $\beta_{IR}(\lambda)$. From the amplitude and phase frequency spectrum described with Eq. (12) one may determine the parameter τ_c. For silicon or gallium arsenide samples the appropriate expression for the plasma component has to take into account the carrier diffusion coefficient as well as the front surface velocity and can be found in Ref. [22] or [H4]. In fact, the plasma component appears also in moderate doped samples not only in undoped or lightly doped samples.

Taking into account formulas (2) and (5), the broadband PTR signal e.g for CdSe can be written as:

$$S_{PTR}(f,\beta,\lambda) = \frac{(1-i)Tt}{\sqrt{2\omega}e(t+1)}\frac{1+M^{-2}(t+1)/(t-1)-2e^{-\beta L}M^{-1}t/(t-1)}{1-M^{-2}} + \frac{C\lambda^2\eta\tau_c}{1+i\omega\tau_c} \quad (13)$$

while for Si and GaAs samples the PTR signal consists of the thermal response (formula (3)) and plasma response (formula (6) in H4).

Apart from photothermal (PT) and photocarrier (PC) response components, the signal can contain also photoluminescence response component. For the semiconductor sample with both sample surfaces polished and etched the expression can be written as follow [H2, H7]

$$S_{PL}(f) \approx \frac{I_0 \cdot \tau}{(1+i \cdot 2 \cdot \pi \cdot f \cdot \tau)} \tag{14}$$

where τ is the lifetime (decay of the photoluminescence).

3. Experimental set-ups and materials

3.1 Experimental set-ups

All photothermal radiometry and lock-in thermography results were carried using the following experimental set-ups. The PTR results reported in H1 were obtained with the experimental set-up presented in Fig. 2.

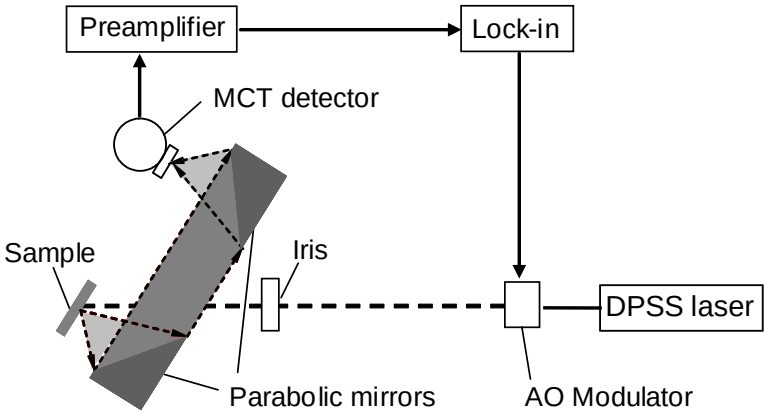

Fig. 2. Modulated photothermal radiometry (PTR) set-up (Reims, France). The iris selects the zero-order diffraction beam. A flat-top beam shaper can be inserted after the iris [H1].

The PTR signal was excited using a DPSS (Diode-pumped solid-state) laser with the output power of I_{cw}=245 mW at the operating wavelength λ=532 nm. The intensity of the laser beam having a diameter of d_{las}=0.7 mm was modulated by means of an acousto–optical modulator (AOM) in the frequency range of 0.1 Hz to 1 MHz. At low frequency, one-dimensional (1-D) heat diffusion was realized by inserting a flat top beam shaper in the laser beam, creating uniform irradiation (7 mm in diameter) over the entire sample surface. Two Au-coated parabolic mirrors captured the IR radiation emitted from the sample, focusing it on a photovoltaic HgCdTe (MCT) detector type KMPV11-1 (Kolmar Technologies) having a sensor diameter of 1 mm and built-in current preamplifier. The detector is cooled by liquid-nitrogen and has an antireflection-coated Ge window which blocks the laser radiation. The wavelength range at half maximum lies between 5 μm and 11.3 μm with the peak responsivity at 9.53 μm (see also Table 1 and Fig. 2). The signal from the detector was processed by a lock-in amplifier type SR850 (Stanford Research) between 0.1 Hz and 100

kHz, and type EG&G 5302 between 100 kHz and 1 MHz. Amplitude A and phase φ frequency scans were acquired and analysed by a PC computer.

All PTR signals were normalized using the transfer function of the set up (measured with a photodiode) below 1 kHz and by the signal from a polished steel sample above 1 kHz. The latter normalization is equivalent to extracting a slope of $f^{-1/2}$ from the amplitude and to adding 45^0 to the phase of measured signals. The resulting spectra are described by Eq. (10). The whole procedure cancels instrumental non-linearity at low and at high ends of the frequency range. Table 1 contains the description of the used IR filters.

Table. 1. Characteristics of IR band pass filters used and calibration factors for two sample temperatures. (*) - filters combined with sapphire window [H1].

Filter	FWHM transmission range (nm)	Effective center wavelength λ_{eff} (μm)	Pass band $\Delta\lambda$ (nm)	Calibration factor (26^0C)	Calibration factor (80^0C)
F33*	2250-3810	3.31	1560	0.0029	0.0083
F50*	3750-5800	5.02	2050	0.0043	0.0090
F61	5510-6700	6.17	1190	0.098	0.12
F72	7060-7400	7.22	340	0.039	0.040
F86	7700-9400	8.63	1700	0.29	0.26
F91	8250-9980	9.14	1730	0.27	0.23
F99	8050-13850	9.89	5800	0.44	0.36

The other PTR results were measured on the self-build by the author experimental set-up which is presented in Fig.3.

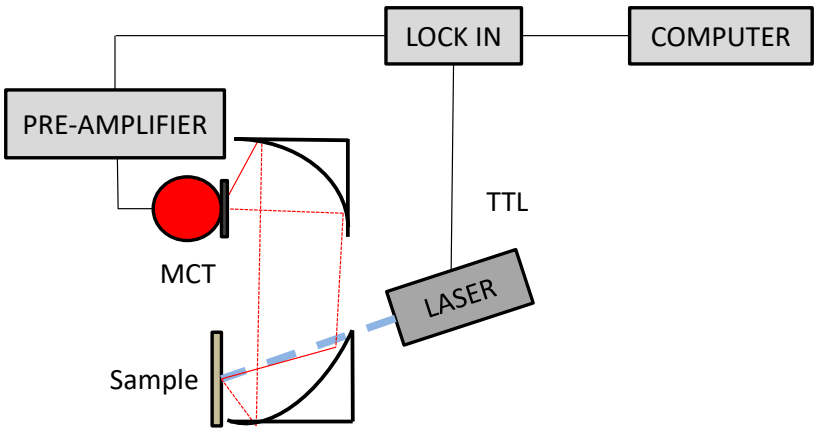

Fig.3. Experimental modulated photothermal infrared radiometry set-up (my laboratory in Torun) [H2]. The results obtained in H7 were acquired with different MCT detector.

The modulated photothermal infrared radiometry signal was excited using a diode laser (Omicron Laser) with the output power of I=150 mW at the operating wavelength λ=405 nm.

The laser beam diameter was $d = 1.24 \pm 0.02$ mm (in H2-H4) and $d \approx 1.5$ mm (in H5-H8 and H9). The intensity of the beam was electrically modulated in the frequency f - range between 40 Hz and 100 kHz by a rectangular (0 – 100%) modulation with 1:1 duty cycle. Two Au-coated off-axial parabolic mirrors captured the emitted IR radiation from the sample, focusing it on a photoconductive MCT detector type J15D12 (Teledyne Judson Technologies) with its detectivity peak at the wavelength of 11.3 μm and with an 1 mm^2 active area (in H7 a detector type KMPV11-1 (Kolmar Technologies) was used). The detector was cooled by liquid-nitrogen and and was equipped with a ZnSe window. Additionally, in order to block the laser radiation, an antireflection-coated Ge window was used. The signal from the detector was processed by a lock-in amplifier SR850 (Stanford Research). The amplitude A and phase φ frequency scans were acquired and analyzed by a personal computer. The samples were placed on the designed aluminum sample holder, which has a smaller hole than the sample diameter, which allows to heat the samples only to about 30-34 ºC. Table 2 contains the description of used IR filters.

Table 2. IR filters and windows in the detection range of the detector [H2a].

Filter/window	Central Wavelength (nm)	Spectral range (nm)	Pass band Δλ (nm)
Infrasil Window	-	2000-4000	2000
MgF_2 Window	-	2000-6000	4000
F35	-	3000-5000	2000
F6	6200	5585-6805	1220
F78	7850	7670-8000	330
F83	8235	7990-8440	450
F87	8688	8545-8745	200
F91	9127	8900-9395	495
F9	9395	7800-9395	1595
F10	10500	9650-11250	1600

Figure 4 presents the schematic diagram of lock-in thermography set-up in the transmission configuration. It consists of an excitation source, the investigated sample and the infrared camera, which collects the infrared signal resulting from the rear part of the irradiated sample. In this experiment, the lock-in detection method was employed to determine the infrared absorption coefficient and the thermal diffusivity of the sample. This means that the amplitude and phase of the signal is detected at a known excitation frequency and rejects signals with other frequencies.

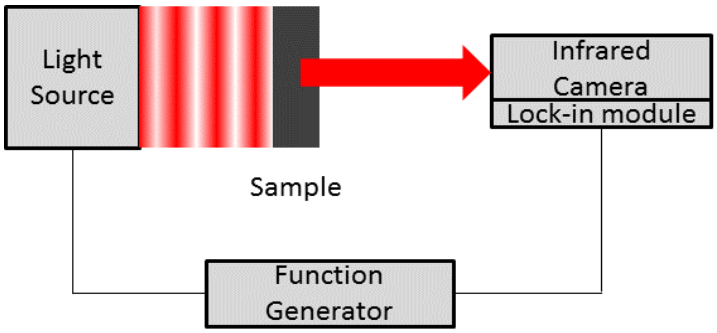

Figure 4. Infrared lock-in thermography in the transmission configuration (Cluj-Napoca, Romania).

The excitation source was a white (400-750 nm) high power light emitting diode panel with an area of 40x40mm^2 and a maximum output power of P_{max}=100W. In our experiment, the modulation frequency was varied between 5 Hz and 100 Hz. Above 100Hz, the infrared images were very noisy. The emitted infrared radiation was recorded using an infrared camera (FLIR 7200 series) having a 256x320 pixel array of InSb (indium antimony) detectors, which are sensitive in the range 1.5 - 5.1 μm. The optical axis of the camera was set perpendicular to the investigated surface.

3.2. Materials

The first group of the studied materials (Si, GaAs and AlGaAs) belong to the most frequently used semiconductors. The second group of investigated materials were ZnTe:Cr, ZnSe:Cr and CdSe which have promising potential applications in infrared optoelectronics. Some parameters of investigated samples are given in Table 3 and 4.

Table 3. Some major characteristics of the investigated heavily and moderate doped samples.

Sample number	Material	Dopant	Type	Carrier concentration N (cm^{-3})	Growing Method
S1	Si	Arsenic	n	1.12x10^{19}	Czochralski
S2	GaAs	Zinc	p	1.10x10^{19}	Vertical gradient freeze
S3	GaAs	Zinc	p	1.10x10^{19}	Vertical gradient freeze
S4	GaAs	Zinc	p	1.10x10^{19}	Vertical gradient freeze
S5	Si	Boron	p	1.16x10^{17}	Czochralski
S6	GaAs	Silicon	n	1.70x10^{18}	Vertical gradient freeze
S7	CdSe	-	n	1.40x10^{17}	Modified vertical Bridgman (Toruń)
S8	CdSe	-	n	0.30x10^{17}	Modified vertical Bridgman (Toruń)
S9	ZnTe	Chromium	-	Not measured	Modified vertical Bridgman (Toruń)
S10	ZnSe	Chromium	-	Not measured	Modified vertical Bridgman (Toruń)

The electrical measurements were performed using Hall set-up [H4]. Samples S1-S6 were polished at one surface, while the other surface remained unpolished. For samples S7-S10 both surfaces were polished and etched. All signals were recorded from the polished surface.

The $Al_{0.33}Ga_{0.67}As$ thin films were grown using the MBE method [H6, H8].

Table 4. Some properties of $Al_{0.33}Ga_{0.67}As$ thin films grown using the MBE method (H6, H8).

Parameter	$Al_{0.33}Ga_{0.67}As$	$Al_{0.33}Ga_{0.67}As$:C	Comments
L_1 (μm)	1.71 ± 0.03	1.81 ± 0.03	SEM images in H6 and H8
$\beta_{opt,1}$ x 10^6 (1/cm)	0.5		Ref. 23
R	0.4		Optical reflection coefficient, Ref. 23
k_1(W/mK)	11.7	10.8	In the case of doped sample the value is 10 % smaller than value for undoped sample taken from Ref. 24
α_1 x 10^{-6} (m^2/s)	6.5	5.85	In the case of doped sample the value is 10 % smaller than value for undoped sample taken from Ref. 24
$\beta_{IR,1}$ x 10^6 (1/cm)	0		C-V measurements
Doping concentration (cm^{-3})	Not doped intentionally	1.3×10^{18}	Concentration of undoped sample was measured using C-V method [H6], while estimation of the doped sample is described in H8
R_{th} (m^2K/W)	$1.5x10^{-9}$		Ref. [25]

4. Experimental results

The broadband, integral PTR results for the CdSe sample (S7) measured without filters and the best fits using Eq. (13) are shown in Fig. 5. To compare with Eq. (13), the normalized experimental amplitudes were divided by $f^{1/2}$, and 45° was subtracted from the normalized phases. The frequency scans were generated by joining three curve sets. Below 10 Hz the measurements were made with the flat top beam shaper to assure 1-D heat flow perpendicular to sample surface. Above 10 Hz the laser beam radius is larger than the thermal diffusion length and the 1-D approximation is satisfied even for the normal beam size (~0.7 mm). Between 100 kHz and 1 MHz the measurements were carried out with the EG&G 5302 lock-in instrument.

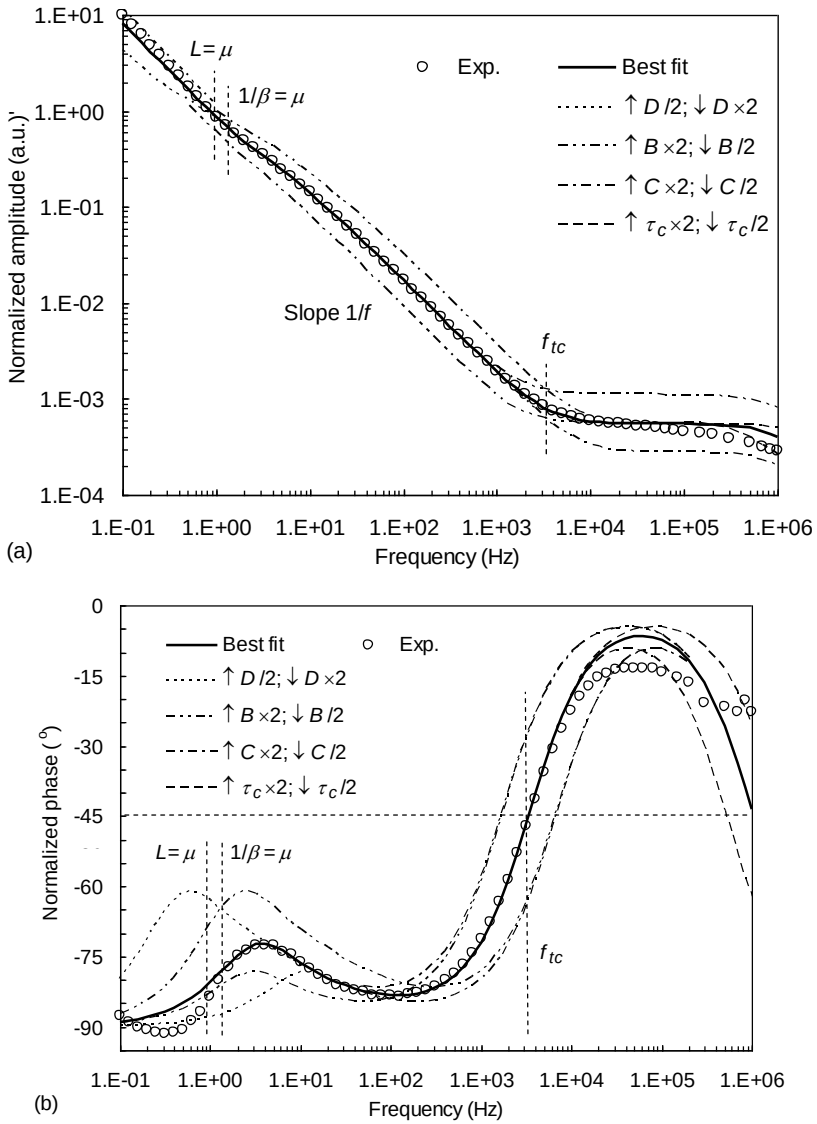

Fig. 5. Experimental (open circles) PTR amplitude (a) and phase (b) for the CdSe sample (S6) measured without IR filter. The full lines represent the best fit of Eq. (13) to experimental data. Broken lines show the sensitivity of the fit to changes of one fit parameter while keeping the best fit values for the other parameters. The markers indicate thermal, thermo-optical and thermal-to-photocarrier wave transition frequencies. Apart from constant factors, Eq. (5) contains only two independent parameters: $B = \beta_{IR}(\alpha/\pi)^{1/2}$ and $D = L/(\alpha/\pi)^{1/2}$. With these intrinsic fit parameters, one may express the combinations of material parameters as $\beta_{IR}\mu = Bf^{-1/2}$, $L/\mu = Df^{1/2}$ and $\beta_{IR}L = BD$ [H1].

In the low frequency range (10 Hz - 1 kHz) the amplitude of the PT component has an slope of about f^{-1} and the phase tends to -90°. This is typical for the thermal PTR signal of a homogeneous, thermally thick and thermo-optically semi-transparent sample ($\beta\mu$<1). The deviations from the fit below 1 Hz are due to heat losses to the ambient. The PC component is manifested in the high frequency range above 10 kHz. The flat amplitude and the phase approaching 0° of the fit curve corresponds to the a non-diffusive regime with negligible surface recombination velocities. The experimental points have a small $f^{-0.11}$ amplitude slope and are by 7° to 10° below the theoretical phase, which might be due to contribution of other lifetimes into the signal as discussed in H1 (see Fig. 6 in H1).

In order to prove the uniqueness of obtained parameters, Fig. 5 also shows numerical simulations using formula (12) for different values of intrinsic fit parameters. Simulations are plotted for parameters which were by a factor of two larger or smaller than the best fit values. At low frequencies the PTR signal is sensitive to changes of the parameter D (containing α), while at intermediate frequencies it is sensitive to parameter B which contains β and a.

The phase is sensitive to τ_c starting from 10 kHz, while the amplitude does so from 100 kHz. As expected for semiconductors, when τ_c decreases (increases) the maximum in phase signal shifts to higher (lower) frequencies respectively. Fig. 6 shows that the set of intrinsic parameters is uncorrelated, meaning that they can be determined independently and with sufficient sensitivity if the frequency dependence of the phase is available in the whole modulation frequency range. With increasing frequency, the phase decreases as most probably the PC component becomes dominant. The PC radiation in the IR range is due to the emission of the plasma wave Δn. For high β_{VIS}, the PC component originates from a shallow depth below the surface with a thickness equal to the carrier diffusion length.

4.1 Influence of the infrared absorption coefficient on estimation infrared absorption coefficient and thermal diffusivity of bulk samples

In the PTR phase in Fig.5 a maximum was observed. The effects of the infrared absorption coefficient, thermal diffusivity and a thickness of the samples on this maximum in the PTR phase were investigated in Ref. H4. In order to meet the requirement of the one-dimensional heat diffusion propagation condition ($d>>|1/\sigma_t(f)|$), the silicon samples were analyzed above 200 Hz, while the GaAs samples were analyzed above 40 Hz, respectively. Figure 6 presents the best fits of the thermal component of formula 3, to experimental data, normalized for the n-type Si and p-type GaAs wafers. To compare with Eq. (6), the normalized experimental amplitudes were divided by $f^{1/2}$, and 45° was subtracted from the normalized phases.

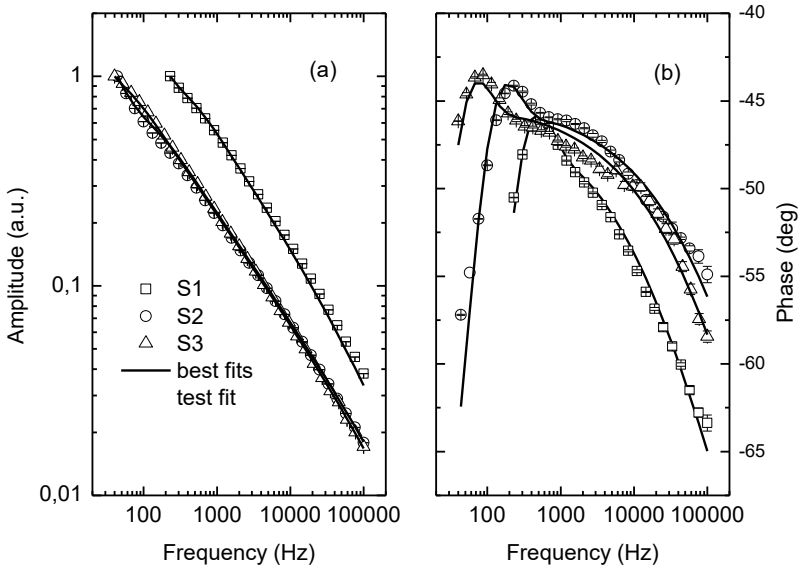

Fig. 6. Normalized modulated PTR amplitude (a) and phase (b) with the best fits using formula 6 for the samples Si (S1,□), GaAs (S2, ○ and S3, Δ, respectively). The estimated parameters for the samples are collected in Table 5. The quality of fitting (determination coefficient/goodness) of the fit are R^2=0.99, R^2=0. 95, and R^2=0.98, respectively [H4].

For highly doped samples the modulated photothermal infrared radiometry (PTR) signal is dominated in the whole range of frequency by the thermal component and the signal strongly depends only on two parameters: the effective infrared absorption coefficient and thermal diffusivity of the sample. Normalized amplitudes and phases of the thermal component deduced from the theoretical model, Eq. 3, predict very well the experimental values. From Figure 6 one can conclude that the PTR phase maximum is shifted (for samples with the same thicknesses) to higher frequencies for the better thermal conductor (silicon is better thermal conductor than gallium arsenide, see Table 3). Moreover, one can also conclude that for the material exhibiting the same thermal diffusivity, the PTR phase maximum is shifted to lower frequencies for the thicker sample (see the thicknesses of GaAs wafers in Table 4). The test fit curve is marked by the dashed line, and the solid lines are the best fits. The experimental results for samples Si (sample S5) and GaAs (sample S6) can be found in H4. Due to the fact that in Si and GaAs samples the carrier diffusivity as well surface recombination velocity cannot be neglected the different equation for the plasma component was used in the model (see comment below eq. 12). The expression given in Ref. 23 was taken for the calculation. The resulting materials parameters are collected in Table 5. Fig. 7 presents the best fits of the model to normalized data for moderately doped samples (S5 and S6).

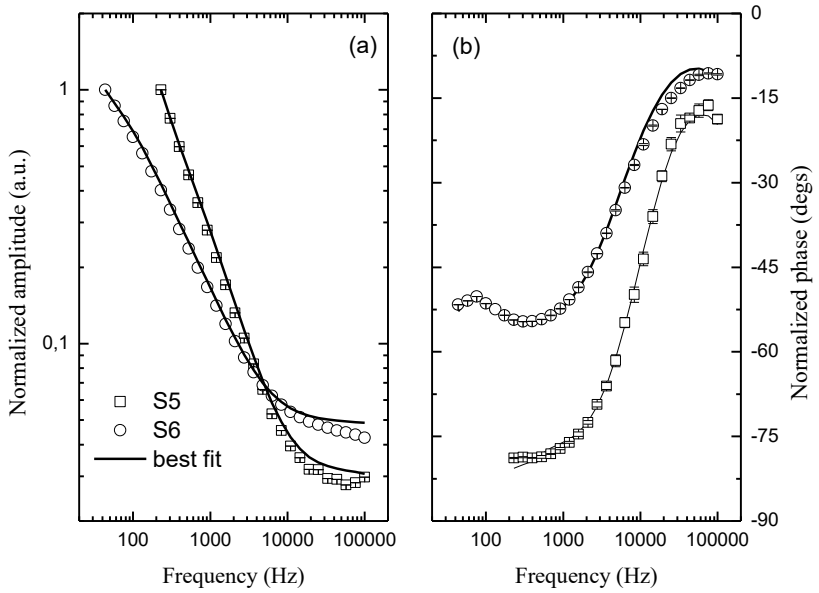

Fig. 7. Normalized modulated photothermal infrared radiometry amplitudes (a) and phases (b) with the best fits using Eq. (6) in H4 for the sample S5 (□) and S6 (○). The estimated parameters are gathered in Table 5. Parameter set as constant: S2 = 10^5 cm/s (unpolished surface). The goodness of the fits were R2 = 0.99. The test fit is marked by the dashed line, the solid lines are the best fits [H4].

The expanded uncertainties with 0.95 level of confidence *U*, given in Table 5, are calculated using the Matlab function *nlparci*.

Table 5. Effective infrared absorption coefficient β_{IR}, thermal diffusivity α and electronic transport parameters (τ is the carrier recombination lifetime, D is the carrier diffusivity and surface recombination velocities S_1) of investigated samples [H4].

		β_{IR} (cm^{-1})	L (cm)	$\beta_{IR} \cdot L$ (1)	α (cm^2/s)	τ (μs)	D (cm^2/s)	S_1 (cm/s)
S1	Si	1100±40	0.041	45.00	0.79±0.04	-	-	-
S2	GaAs	4000±400	0.040	160.00	0.27±0.01	-	-	-
S3	GaAs	3600±300	0.065	234.00	0.27±0.01	-	-	-
S5	Si	19 ±2	0.041	0.78	0.70±0.20	0.5±0.2	16±4	110±40
S6	GaAs	150±10	0.063	9.70	0.25±0.03	0.2±0.1	10±2	1200±200
S7	CdSe	15.3±1.5	0.120	1.83	0.048±0.004	0.15±0.03	-	-
S8	CdSe	5.15±0.50	0.120	0.62	0.047±0.005	0.010±.005	-	-

The values of the thermal diffusivity for the Si samples (samples S1 and S5) agree with the literature values for silicon (0.88 cm^2/s) [26] and for GaAs samples (samples S2 and S3) with the value reported for GaAs (0.31 cm^2/s) [27]. Moreover, the values of the thermal diffusivity of CdSe samples agree well with values obtained using photopyroelectric method [28]. This can be considered as a confirmation of the proposed theoretical approach. Slightly lower values of thermal diffusivities obtained in this work are attributed to the fact that with increasing doping, the thermal conductivity of the samples decreases due to enhanced phonon scattering [29, 30] and the increasing temperature during measurements (increase up to ~34 °C in results for sample S1-S6 and ~30 °C(measurements with the top flat beam). As one can notice, the thermal diffusivity can be derived with a different precision. The highest precision (the lower relative expanded uncertainty U_r = 0.05) is obtained for the samples where the signal contains only a thermal response (samples S1, S2 and S3). When photocarriers also contribute to the PTR signal, then the uncertainties of thermal diffusivity estimation increases. Here, it is worth discussing the influence of the thermal, infrared, geometrical (thickness) and carrier recombination properties of the sample on the existence of the PTR phase maximum. The PTR phase maximum can be only present in the thermal response, and its position depends on thermal diffusivity and thickness of the sample (Fig. 6). It is clearly seen that PTR phase maxima are observed for samples in which $\beta_{IR} \cdot L > 1$. For highly IR absorbing samples (S1, S2 and S3), the thermal response dominates over the whole modulation frequency range (Fig. 6) due to large values of the infrared absorption coefficient (Table 5). For moderate doped samples, the thermal response dominates only at low modulation frequencies (Fig. 5). It is very interesting to compare the results for the Si (sample S5) and CdSe (sample S8) samples. For these samples $\beta_{IR} \cdot L < 1$, but the PTR phase maximum is only observed for the CdSe sample (S8). This is because, the CdSe sample has much worse thermal properties in comparison to silicon samples, and the sample S8 is thicker than S5. As one can conclude (based on the results obtained for silicon (S1) which has almost the same thickness), the PTR phase maximum for Si sample (S5) is expected to be around 630 Hz. For this frequency, the transition between thermal and plasma response already began. The transition frequency from the thermal to plasma response depends, in turn, on the carrier recombination properties of the sample. The longest recombination lifetime is the transition between thermal and plasma response beginning at lower modulation frequencies of the PTR signal. Fig. 8 presents the correlation between the ratio α/L^2 and the frequency of the PTR phase maximum.

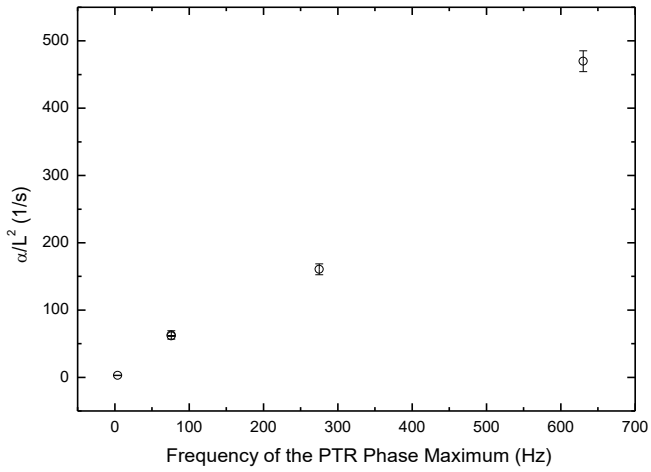

Fig. 8. Correlation between the α/L^2 and the frequency of the PTR phase maximum. The errors of the maximum frequencies are smaller than the points presented in this figure [H4].

The results presented in Fig. 8 confirm the conclusion that the PTR phase maximum is shifted to lower frequencies for the thicker samples exhibiting the same thermal properties. This conclusion can be very useful for improving the accuracy of the estimation of the thermal diffusivity for some kind of the samples, eg. like Si sample (S5) in our work.

Finally, the precision of estimation of the infrared absorption coefficient of the sample is not depending on the value of of the infrared absorption coefficient and it equals to 10%.

4.2.Methods of estimation infrared absorption coefficient applied bulk samples.

The first method, relies on measurement of the infrared absorption coefficient of the sample from the PTR amplitude described detailed in H1. For some frequencies and materials the PTR amplitude is proportional to the infrared absorption coefficient:

$$S_{PT}(f,\beta_{IR}) = \frac{(1-i)T_a}{\sqrt{4\pi f e}} \frac{\beta_{IR}\mu}{\beta_{IR}\mu + 1 + i} \approx \frac{-iT_a\beta_{IR}}{2\pi f \rho c} \qquad (15)$$

T_a is the instrumental constant and ρc volumetric heat capacity. In order to use formula (14) the following requirement must be fulfil: the sample is thermally thick relative to its thickness ($L>\mu$, $M>1$) and also relative to the optical penetration depth, $1/\beta_{opt}\geq\mu$. Then the last factor in formula (14) is close to unity. Last approximation is valid for $\beta_{IR}\mu<1$. It indicates that $|S_{PT}|\propto\beta_{IR}/f$ (experimentally it is usually for lightly absorbing sample $f^{0.9}$) and that the phase is saturated to φ=-90^o. However, due to the fact that the absolute value of the PTR amplitude is not know the infrared absorption coefficient is determined using the following procedure:

1) Estimation of the effective infrared absorption coefficient of the sample using broadband and integral (without IR filters) PTR measurements (see Fig. 6 and table 5),
2) Measurement of the PTR amplitude for the used IR filter specified in table 2 and calculation the ratio relative to the amplitude curves measured without filter. The absolute scale was set by taking the effective infrared absorption coefficient.
3) Obtained values of the infrared absorption coefficient were additionally divided by the filter calibration factors which minimized effects of the sample temperature and sensitivity of the detector (for details see section III.C in [H1]).

The second method, relies on simultaneously fitting parameters of the model described by formula (3) to experimental amplitude and phase. In front of the detector the IR filters were placed (spectrally resolved measurements, SR-PTR). Figure 9 presents the best fits of the theoretical model described by formula (3), to normalized experiment data of GaAs sample (S4) measured using selected IR filters specified in Table 2.

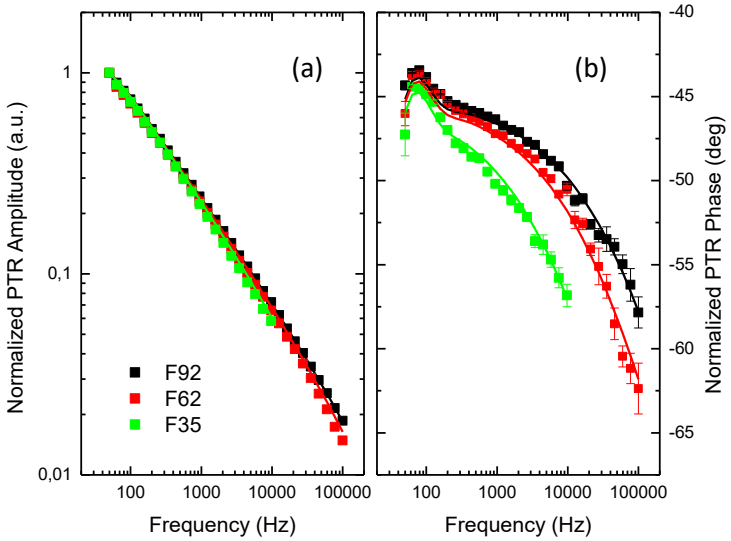

Fig. 9. Normalized photothermal infrared radiometry amplitude (a) and phase (b) signal with the best fits using formula (3) to the experimental data for the *p*-type GaAs wafer measured with the IR filters placed in front of the detector [H5].

It is worth pointing out that the PTR phase is more sensitive than the PTR amplitude to changes of the infrared absorption coefficient. Further, from Fig. 9, it can be concluded that the PTR phase is more sensitive for changes of the infrared absorption coefficient at higher modulation frequencies than at lower frequencies. Table 6 presents estimated values of thermal diffusivity and infrared absorption coefficient of GaAs:Zn (sample S4).

Table 6. Infrared absorption coefficients and thermal dyffusivities of the sample GaAs:Zn [H5, 30].

IR filtr	Spectral range (nm)	β_{IR} (cm^{-1})	α (cm^2/s)
F35	3000-5000	1300± 200	0.26±0.03
F62	5585-6805	2500 ± 300	0.26±0.02
F78	7670-8000	3450 ± 500	0.26 ±0.02
F83	7990-8440	3600 ± 500	0.26 ±0.02
F87	8545-8745	4200 ± 600	0.27 ± 0.02
F92	8900-9395	3800 ± 300	0.27 ± 0.02
F105	9650-11250	3600 ± 200	0.27 ± 0.02

It is worth mentioning that for all IR filters the same value of the thermal diffusivity of GaAs:Zn which demonstrates that SR measurements increase the reliability of estimating of thermal diffusivity of the samples. From results presented in Fig. 9a and Table 6 indicate that the slope of the amplitude drop is related with the infrared absorption coefficient. The third

method is based on the measurement of the slope of the PTR amplitude. One can prove that $|PTR| = a \cdot f^n$ where a is constant. This formula is valid at enough high frequencies. Furthermore, the slope (parameter n) can vary between -0.5 and -1 depending on the infrared properties of the sample: $f^{-0.5}$ for IR opaque samples and as f^{-1} for IR transparent samples. Taking into account that $\beta_{IR} \rightarrow 0$ for IR transparent samples and $\beta_{IR} \rightarrow \infty$ for IR opaque samples, the infrared absorption coefficient can be expressed using the semi-empirical formula:

$$\beta_{IR} = C_1^n \tag{16}$$

where C_1 is constant. Fig. 10 presents the correlation between the steepness parameter n and the effective infrared absorption coefficient β_{IR} calculated using the computational method reported earlier in Ref. H4 and Table 5.

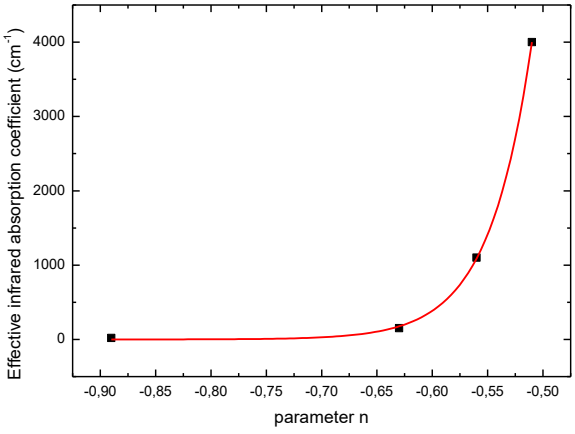

Fig. 10. Correlation between the steepness parameter n and the (effective) infrared absorption coefficient β_{IR} for the investigated samples [H9].

Using formula (16) the experimental points in Fig.10 can be adjusted to the semi-empirical formula:

$$\beta_{IR} = 2.31 \cdot 10^9 (1.98 \cdot 10^{11})^n, cm^{-1} \tag{17}$$

It can be shown that the method can be also applied for the determination of infrared absorption coefficients using SR-PTR data [H9]. This is because the effective infrared absorption coefficient measured by PTR is a valuable fingerprint of the IR properties of sample in a defined spectral wavelength interval which can be used if high spectral resolution is not required. It was proven that calculated values of the effective infrared absorption coefficients using formula (7) from infrared absorption coefficients estimated using the PTR method (Fig. 11) and measured values of two CdSe samples are in very good agreement (please see Table 2 in H9). The infrared absorption coefficient of the sample S4 (GaAs:Zn) was also determined using the third method (Fig.12).

For the investigated CdSe samples the infrared absorption coefficients were calculated using first method. The requirements for the approximations in formula (14) are met above 4 Hz. The $\beta_{IR}(\lambda)$ values are calculated at 80 Hz (for sample S7) and at 10 Hz (for sample S8). Figure 11 shows the comparison of estimated values of the infrared absorption coefficient of samples S6 and S7 with the infrared absorption coefficients measured using FTIR method in the transmission configuration [31].

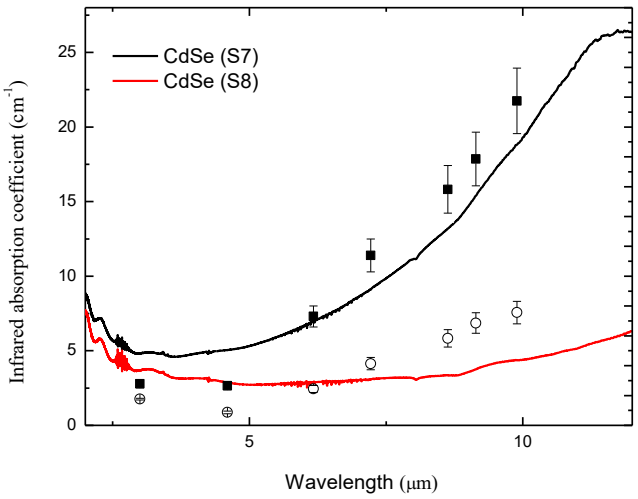

Fig. 11. IR absorption coefficient $\beta(\lambda)$ from PTR measurements (open circles and full squares) and from FTIR transmission spectra (solid curves), for the two CdSe samples. Error bars lead to ±10 % estimated accuracy of absolute beta values [H1].

The qualitative agreement is satisfactory, and the differences can be explained as follows. The computation of $\beta_{IR}(\lambda)$ from the FTIR spectrum relies on the inversion of the expression of the transmittance of a sample slab taking into account multiple internal reflections [31]. This expression requires the knowledge of the reflectance at the sample/air interface R which in turn, depends on the refractive index n_r = 2.43 - 2.5 [32]. With this, $R = [(n_r - 1)/(n_r + 1)]^2$ = 0.17-0.18 in the IR range. The error upon the inversion of the transmittance formula diverges for high transmission. In practice, $\beta_{IR}(\lambda)$ spectra derived from transmission spectrophotometry have low accuracy when the optical thickness $\beta_{IR}L < 0.2$, or when β_{IR} is lower than a few cm^{-1} for the investigated samples. This limit concerns the baselines of the FTIR spectra of Fig. 11. On the other hand, $\beta_{IR}(\lambda)$ was derived from the PT signals without taking into consideration the internal reflections within the sample. In the front-detection PTR configuration, if considering a double optical path within the sample (a single reflection R at the rear side), in the worst case the lowest $\beta_{IR}(\lambda)$ values decrease by 17-18 % compared with the obtained vales at Fig.11. This corresponds to the R values computed above and is valid for low $\beta(\lambda)$ values, between 4 Hz and f_{tc}. The correction of $\beta_{IR,eff}$ estimated for CdSe samples has to be made only for sample S8 (-4.5 %). As a result, the points situated below ≈5 cm^{-1} in Fig. 11 are in fact lower by ≈5-15 %. Overall, one may state that spectrophotometric methods based on absorption measurements (like PTR) are more accurate than those based on transmission measurements (FTIR) for samples with low optical thickness ($\beta_{IR}L << 1$). In addition, measurements with the PTR method can reveal a depth dependence of the IR absorption whereas conventional FTIR delivers a depth-averaged value and it can also effect the obtained results.

However, both spectra show the increase of the infrared absorption coefficient with the increasing wavelength (absorption on the free carrier) which can be described by Drude theory [34]

$$\beta_{IR}(\lambda) \sim \lambda^2 N, \tag{18}$$

where N is the carrier concentration. The observed character of the dependence of the infrared absorption coefficient on the wavelength of the absorbed radiation is rather of the type $\beta(\lambda) \sim \lambda^p$, where $1.5 < p < 3.5$. Although the samples have temperature near ~80ºC, it was found that temperature has very weak influence above room temperature on carrier concertation CdSe (S7) [35] thus (based on formula (18)) on the infrared absorption coefficient.

In turns, the infrared absorption coefficients in GaAs:Zn were calculated using the second method. Fig. 12 presents the absorption coefficients calculated from the FTIR reflectance using the Kramers-Kronig (KK) formalism (for more detail please see H5) for zero reflectance outside the measured region (solid blue) and constant reflectance outside the measured region (black-dashed). In addition, Fig. 12 also presents the infrared absorption coefficients measured using the PTR method (black squares).

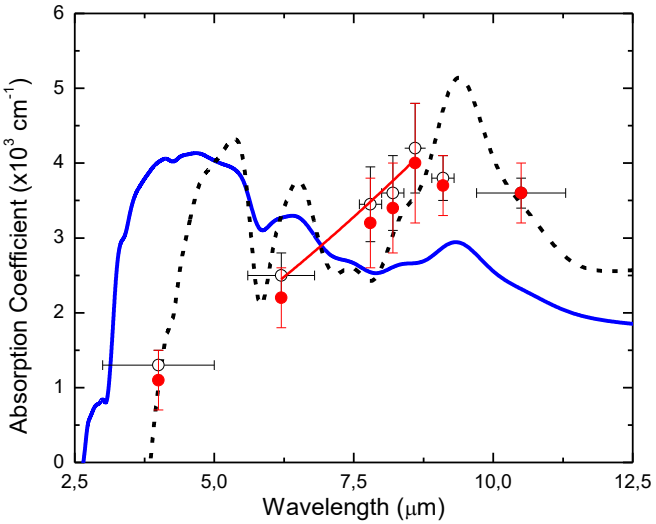

Fig. 12. The infrared absorption coefficient calculated as a function of wavelength in the infrared regime of the electromagnetic spectrum (in solid blue, for zero reflectance outside the measured region, while in black-dashed – for constant reflectance outside the measured region). For comparison, the infrared absorption coefficient measured by the PTR method (open circles) is plotted calculated using the computational methods. The solid red line emphasizes the increase of the infrared absorption coefficient as a function of the wavelength. In turns the red circles presents the infrared absorption coefficient calculated using the semi-empirical method [H5].

At shorter wavelengths, the FTIR results show the maxima of the infrared absorption coefficient as a consequence of the transitions from the heavy- and light-hole to the split-off hole band. This effect has been already observed in 2 μm thick *p*-GaAs films, however, the magnitude of this effect is several times higher than reported in Ref. 36. The use of IR filter F35 in the PTR method, covering a relatively broad range of the spectrum (3-5 μm) is probably masking the maximum that is otherwise observed in FTIR method. At longer wavelengths, the infrared absorption coefficient spectrum estimated using PTR method shows a monotonic increase with increasing wavelength. It is a typical signature for free carrier absorption in materials. The estimation of the scattering mechanism coefficient p ($\beta_{IR} \sim \lambda^p$) yields a value of 1.5. This suggests that the dominating scattering mechanism is related to the scattering of the holes on the acoustic phonons. This value is in a good agreement with experimental results obtained on 2 μm thick Be-doped *p*-type GaAs sample (2.5 x 10^{19} cm^{-3}), reported in Ref. 36. The FTIR results also present the monotonic increase of the infrared absorption coefficient with increasing wavelength. However, firstly we note that this effect is barely seen for the infrared absorption coefficient spectrum calculated using the assumption

that the reflectance outside the measured region is constant. Secondly, for infrared absorption coefficient spectrum calculated using assumption that the reflectance outside the measured region is zero the scattering mechanism parameter p is above 4 (the physical limit of the scattering mechanism parameter is limited by impurity scattering where p = 3.5). Above 9 μm, the infrared absorption coefficient estimated using PTR method decreases with increasing wavelength. This in turn is caused by the inter-valence band (IVB) transitions [36,37], which is also observed in the spectra obtained by FTIR method.

4.3. Photoluminescence component in the PTR signal

Here is worth to compare $\beta_{IR}(\lambda)$ spectra (proportional to the PT magnitude, see eq. 14) with the PC magnitude spectra for the sample S7 and S8 in Fig. 13. In the same way, the magnitude values of the PC component are relative to the curves measured without filter (red circles). These values are arbitrarily scaled to the $\beta_{IR,eff}$ values of samples S7 and S8, respectively, allowing for a direct comparison of the PT and PC spectral trends.

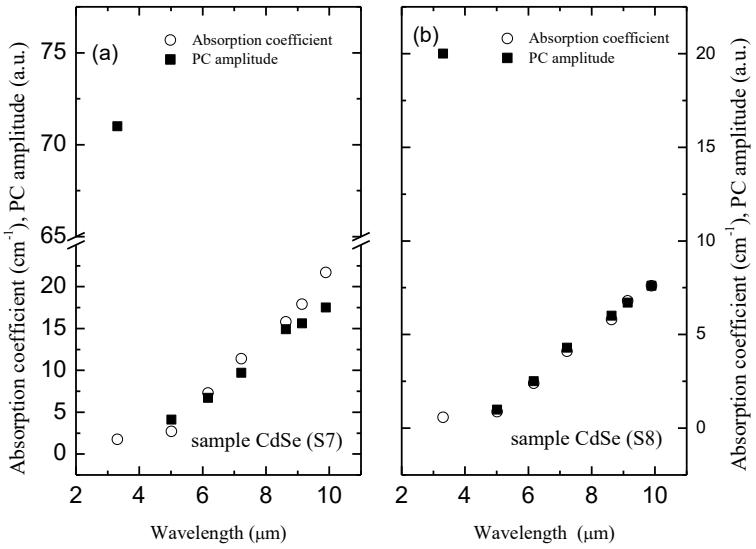

Fig. 13. IR absorption coefficient $\beta_{IR}(\lambda)$ spectra and relative photocarrier (PC) magnitude spectra for CdSe (S7) and (S8) samples. The large values of photocarrier response at 3.31 μm are attributed to photoluminescence (PL) phenomena [H1].

The similarity between the PT and PC components in the range of 5 μm to 10 μm is striking in Fig.13. Theoretically, this implies in formulas (12) and (14) the PC component is proportional to λ^2 and furthermore based on Drude theory (formula(18)) $\beta_{IR} \propto \lambda^2$. In turns based on formula (15) the PT component is proportional to β_{IR} thus $S_{PT} \propto S_{PC}$. The physical reason behind this relation is the equivalence between the emissivity and absorptivity implied by Kirchhoff's law. Thus the mid-IR emission spectrum of the PC component reproduces the absorption spectrum which is apparent in the PT component via the β_{IR} coefficient. This is the first direct experimental evidence of the key assumption in PTR that each de-exciting carrier acts like a blackbody (Planck) radiator.

Fig. 13 clearly shows that the PC amplitude at 3 μm differs noticeably from other values which follow the $\beta_{IR}(\lambda)$ spectra. Plotting in Fig.14 the phase of the signal as a function of modulation frequencies one can observe also that the carrier dynamics is different.

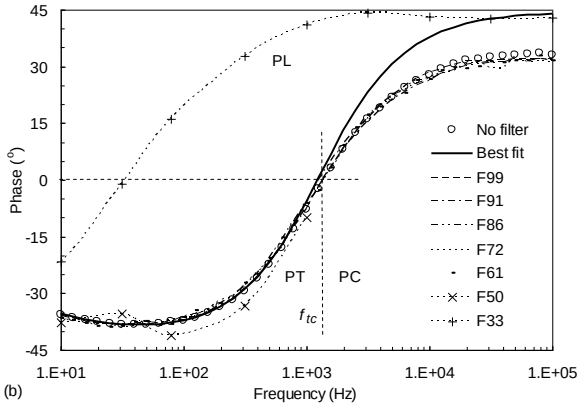

Fig. 14. The PTR phase obtained for CdSe sample (S8) for different filters specified in Table 1. Compared to other figures for the purpose of normalization 45º have been added to the measured phase [H1].

Based on results presented in Fig. 13 and 14 it was suggested that the photoluminescence can also contribute to the PTR signal. For this reason a modified name: modulated infrared radiometry was introduced. To demonstrate the utility of the PTR method for the study of photoluminescence in the mid- infrared range crystals of ZnSe and ZnTe doped with the transition-ion metal chromium were investigated. Figures 15a and b show the spectrally resolved PTR-measurements performed using filters specified in Table 2 of the ZnTe:Cr and ZnSe:Cr crystals, respectively.

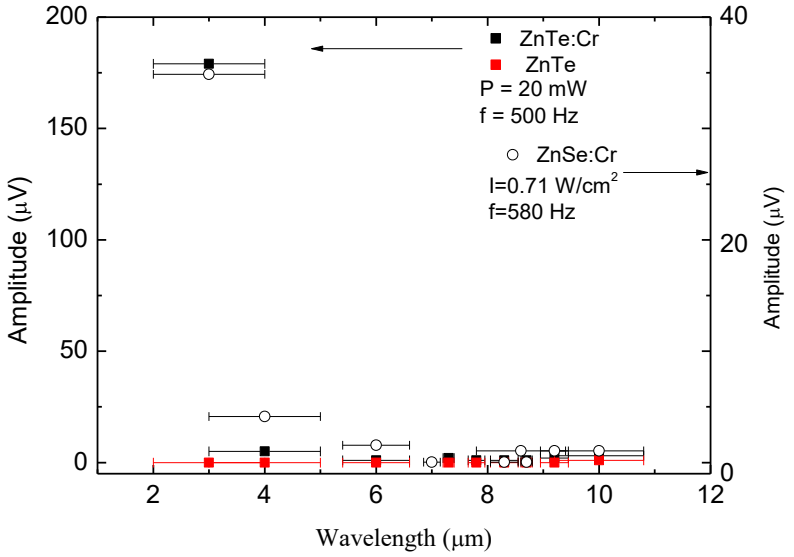

Figure 15. The modulated infrared radiometry un-normalized amplitudes of ZnTe:Cr [H2a] and ZnSe:Cr [H7] measured using a light intensity of 1.7 W/cm^2 and 0.71 W/cm^2 at the modulation frequency of 500 Hz and 580 Hz, respectively.

From Fig. 15 *a* and b one can see that the IR photoluminescence occurs in the wavelength range between 2 and 3 μm for $^5E \rightarrow {}^5T$ transition of Cr^{2+} [38-40]. As, the emission spectra are very broad the poor spectral resolution of used set-up is sufficient enough for the investigation of II-VI semiconductor materials doped with transition metals. Figure 16 shows

the frequency characteristics of the modulated infrared radiometry signal of amplitude and phase of ZnSe:Cr crystal measured with an Infrasil window for different values of the light intensities.

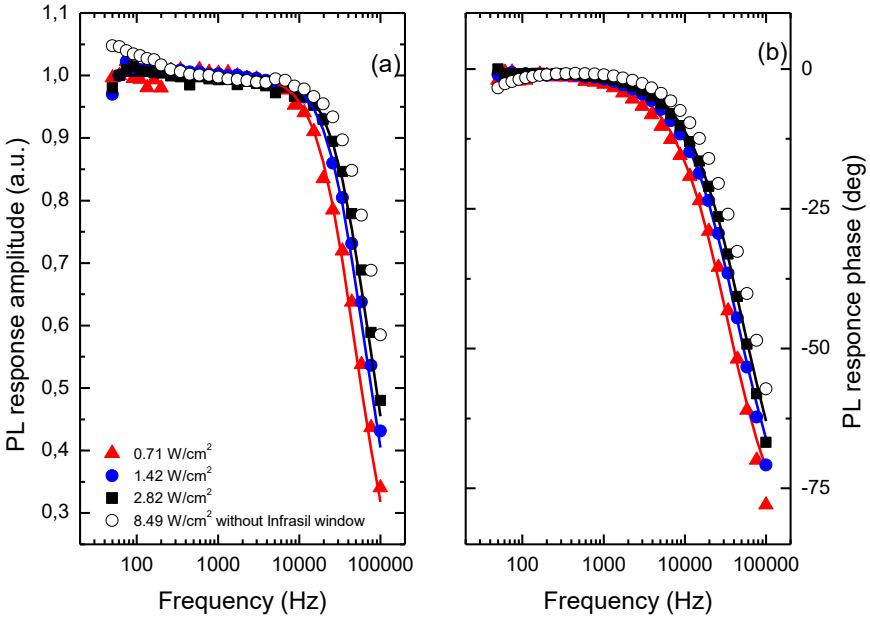

Fig. 16. Frequency-dependence of the amplitude (a) and phase (b) of photoluminesce response of the ZnSe:Cr sample for different light intensities. Points are the experimental data and lines are the best fits to formula (14). The experimental errors are smaller than presents points [H7].

It is worth mentioning that for ZnSe:Cr crystal the modulated infrared radiometry filtered out using the Infrasil window is entirely dominated by the photoluminescence response. When the signal is recorded without Infrasil window (open circles in Fig. 16) a very small photothermal response (or more precisely photothermal to photoluminescence transition) is observed at frequencies below 200 Hz, as expected for the infrared nearly transparent and relatively thin sample. When the light intensity (for measurements with the Infrasil window) increases then the characteristic knee in the amplitude and phase shift to lower frequencies, as expected. Fits of the formula (13), to experimental data are performed using Matlab function *lsqcurvefit*. The obtained recombination lifetimes of ZnSe:Cr crystal are collected in Table 7. Moreover, it must be emphasized that the phase and after self-normalization also the amplitude are not dependent on any proportionality coefficients in formula (14). They are in good agreement with corresponding values reported by other authors (~6.5 μs) [38, 39]. The expanded uncertainties with 0.95 level of confidence *U*, given in Table 7, are calculated using the Matlab function *nlparci*.

Table 7. Measured lifetimes in ZnSe:Cr [H7].

Intensity (W/cm^2)	Lifetime (μs)	R^2	Signal to noise ratio at 100 kHz
0.28	5.5 ± 0.3	0.986	100
0.71	4.7 ± 0.3	0.992	400
1.42	4.1 ± 0.1	0.994	1000
2.82	3.6 ± 0.1	0.996	1500
5.66	3.1 ± 0.1	0.996	3000
8.49	2.9 ± 0.1	0.997	4000

From Table 7 one can see that with increasing laser intensity the lifetime decreases. Noteworthy is the high precision lifetimes measurement and high signal-to-noise ratios at 100 kHz demonstrating the great suitability of the used method for determination of the lifetimes. Since it was demonstrated that the signal contains only the photoluminescence detected in the wavelength range between 2 and 3 μm as a result of $^5E \rightarrow {}^5T$ transition of Cr^{2+}, the measured lifetime is the radiative lifetime of chromium transitions.

Fig. 17 shows the modulated infrared radiometry amplitude and phase measured with and without MgF_2 window of ZnTe:Cr crystal.

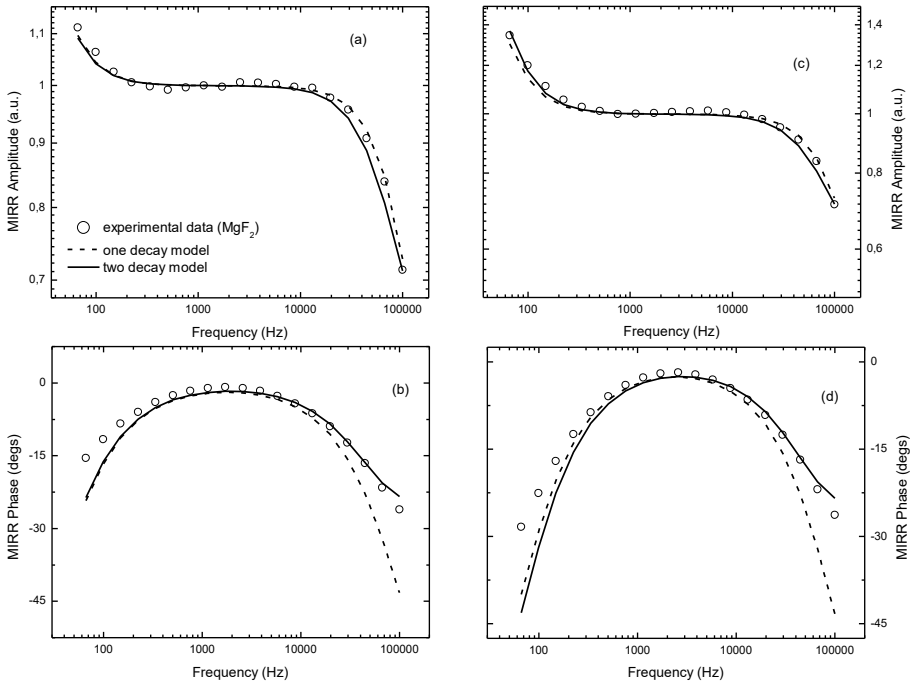

Fig.17. The best fits of the model described by formulas (18) and (19) to the normalized experimental data with (a and b) and without (c and d) the MgF_2 window. The analysis was performed using proposed models for the PL component (dotted line – one decay model, solid line – two decays model) [H2].

Compared to ZnSe:Cr crystal, in ZnTe:Cr crystal the photothermal response is much larger as it is shown in Fig.16 and the (effective) infrared absorption coefficient can be estimated. This means that estimated parameters yield information also about infrared absorption coefficient. The best fits of the models to experimental data showed in Fig. 19 were performed using the following models [H2]:

$$S(f) = T_{ca}\left(\frac{-i\beta_{IR,eff}}{2\pi f \rho C} + B\left(\frac{\tau_1}{1+i2\pi f\tau_1}\right)\right) \qquad \text{for one decay model (19)}$$

$$S(f) = T_{ca}\left(\frac{-i\beta_{IR,eff}}{2\pi f \rho C} + B\left(\frac{\tau_1}{1+i2\pi f\tau_1} + K\frac{\tau_2}{1+i2\pi f\tau_2}\right)\right) \qquad \text{for two decay model (20)}$$

where $\rho \cdot C$ is volumetric heat capacity, T_{ca} is the instrumental constant, β_{eff} is an effective infrared absorption coefficient, B is a weighted coefficient between the photoluminescence to photothermal response. For the normalized amplitudes the model very well predicts the experimental values for both models of the PL component. For the normalized phases there are some deviations between the experiment and the theory at low and high frequencies for one exponential decay model and only at low frequencies for two exponential decay model. Table 8 presents the results of the best fits.

Table 8. Effective infrared absorption coefficient and recombination lifetimes of ZnTe:Cr sample estimated using best fits of formulas (18) and (19) to normalized experimental data [H2].

	One decay model			Two decay model				
Detection range	β_{IR} (cm^{-1})	τ (μs)	B (a.u.)	β_{IR} (cm^{-1})	τ_1 (μs)	B (a.u.)	K (a.u.)	τ_2 (μs)
2-6 μm	1.4	1.5	$5 \cdot 10^5$	1.4	2.3	$1.7 \cdot 10^5$	15	0.15
2-12 μm	2.6	1.5	$5 \cdot 10^5$	3.0	2.3	$1.7 \cdot 10^5$	15	0.15

Moreover, it clearly seen that the two exponential model better predicts the experimental results than the one exponential model. This statement agree with the results obtained by Luo et al. [40]. They analyzed time domain IR photoluminescence from the molecular-beam epitaxy grown ZnTe:Cr layer excited by the laser with the wavelengths 355 nm and 532 nm and also observed two lifetimes : 3 μs and $\tau > 10$ μs. This two exponential PL decays were attributed to indirect excitation of the Cr^{2+} ions. Figure 18 presents data displaying the effect of the light intensity on modulated infrared radiometry signal measured with and without Infrasil window.

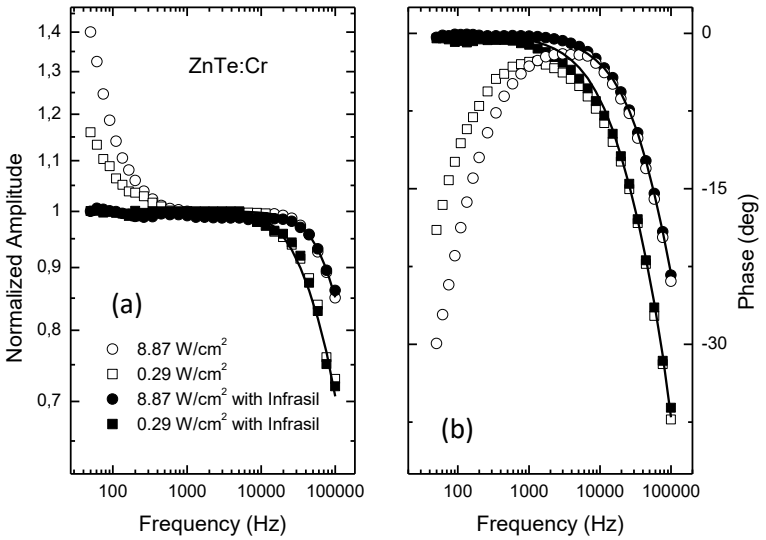

Fig. 18. Effect of the light intensity on modulated infrared radiometry signal from ZnTe:Cr crystal with and without infrasil window measured using detector type KMPV11-1 Kolmar Technologies [H7].

The observed difference of infrared radiometry signals measured for different light intensities at high frequencies can be explained by the change of recombination lifetimes at different light intensities. This effect can also be observed for measurements performed without the Infrasil window. However, both frequency-characteristics are affected by the photothermal response which is described by coefficient *B*. By spectrally limiting of the photoluminescence response using Infrasil not MgF_2 window one can see that the signal which entirely dominated by the photoluminescence response for both light intensities (flat amplitude and no phase lag at low frequencies). If so, the model can be much simplified [H7, 41]

$$S(f) = C\left(\frac{f_1\tau_1}{1+i2\pi f\tau_1} + \frac{f_2\tau_2}{1+i2\pi f\tau_2}\right) = C\left(\frac{\tau_1}{1+i2\pi f\tau_1} + \frac{K\tau_2}{1+i2\pi f\tau_2}\right) \quad (21)$$

where C is a constant, f_1 and f_2 are the corresponding weighting factor for τ_1 and τ_2, $f_1 + f_2 = 1$, τ_1 and τ_2 are the lifetimes and K is the weighting coefficient. Table 9 presents estimated values of the lifetimes and weighted coefficient K for ZnTe:Cr crystal using the expression of the photoluminesce response given in formula 21 and experimental data obtained for infrasil window.

Table 9. Measured lifetimes in ZnTe:Cr [H7].

Intensity (W/cm^2)	Lifetime τ_1 (μs)	Lifetime τ_2 (μs)	Weighted coefficient K (a.u.)	R^2
0.29	1.5 ± 0.1	4.4 ± 0.9	0.07 ± 0.03	0.996
8.87	0.4 ± 0.2	1.5 ± 0.3	0.2 ± 0.1	0.999

For the measurements using MgF_2 window (Fig. 17, Table 8) also two lifetimes were extracted from the experimental data. The obtained lifetimes were slightly different from the values retrieved using Infrasil window. The possible explanation can be that measurements were performed at the different place of the crystal and there is probably some inhomogeneity in the sample. However, the longer lifetime was connected with the infrared emission within Cr^{2+} ions as observed by other authors [40]. Authors investigated a thin ZnTe:Cr film and obtained two lifetimes : one shorter related to the PL decay, while the longer lifetime was attributed to indirect excitation of Cr^{2+} ions. One of the advantage of solely analysis of the photoluminescence response is, that using weighted coefficient K one can estimate contribution of the particular lifetimes into the signal and also the number of unknown parameters is reduced. The calculated contributions (f_1) of the lifetime τ_1 into the signal are 93% for low intensity and 83% for high intensity of illumination, respectively. Based on this finding and data in Fig. 15b, one can conclude that lifetime τ_1 is radiative lifetime of chromium transitions, while τ_2 is probably related with recombination lifetime of photo-carriers due to indirect excitation. Moreover, with increasing light intensity contribution of the infrared PL due to Cr^{2+} emission decreases. Finally, the obtained estimation error of radiative lifetime of chromium transitions is larger for higher light intensity. The advantage of spectrally-resolved over the integral (without filters) measurements is not only effective separation of the photothermal/photocarrier response from photoluminescence response, but also a possibility (depending on the sample properties) to measure the absorption and photoluminescence spectra using one experimental set-up.

4.5 Investigation the thermal and infrared properties of the thin layers

The SR-PTR method can be also used also for measurements of the thermal properties of the thin film. In order to analyze the SR-PTR measurements obtained for the AlGaAs thin films epitaxially grown on heavily doped GaAs substrate the amplitude ratios and phase differences defined as follow were calculated [H6, H8]:

$$Amplitude\_ratios = \frac{Amplitude\_AlGaAs/GaAs}{Amplitude\_GaAs}, \tag{22}$$

$$Phase\_difference = Phase\_AlGaAs/GaAs - Phase\_GaAs. \tag{23}$$

Firstly, the infrared absorption coefficient and thermal diffusivity of GaAs sample using a procedure described in H5 has to be estimated. The procedure relies on the fitting of the one-layer model to the experimental data using Matlab function *lsqcurvefit* with the trust-region-

reflective algorithm used as the minimization algorithm. Secondly, assuming that some of the sample parameters are known a prori one can determine thermal (thermal diffusivity and conductivity of thin film) or infrared of the thin film parameters. This is due to the fact that with all parameters used as fitting parameters the obtained estimation errors are very big. Figure 19 presents the typical best fits of the theoretical model to amplitude ratios and phase differences for undoped $Al_{0.33}Ga_{0.67}As$ alloy and C-doped $Al_{0.33}Ga_{0.67}As$ alloy (open squares) thin films. In the case of undoped $Al_{0.33}Ga_{0.67}As$ alloy, the infrared absorption coefficient of the thin layer and thermal boundary resistance were set constant, and the fitting was performed with thermal conductivity and diffusivity of the thin film as unknown parameters. In turns for C-doped $Al_{0.33}Ga_{0.67}As$ alloy thermal conductivity and diffusivity were set constant and the fitting was performed with thermal boundary resistance and infrared absorption coefficient of the thin film as unknown parameters

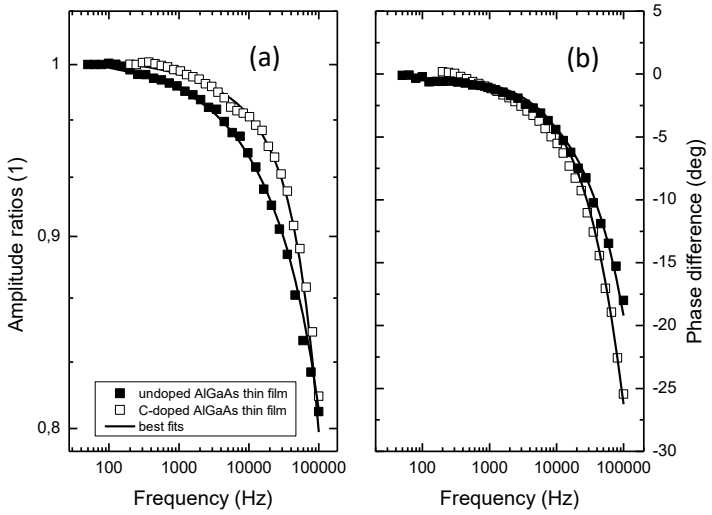

Fig. 19. Amplitude ratios (a) and phase difference (b) as a function of frequency for the undoped and C doped $Al_{0.33}Ga_{0.67}As$ alloys using filter F9 [H8].

It is worth emphasizing that the phase difference at low frequencies (up to about 500 Hz) is very small (less than 1 degree), which means that at low frequencies the PTR signal is emitted from the substrate, as expected. At high frequencies, the PTR signal yields information about the thin film. Besides, it can also be observed that at the frequency of 100 kHz the PTR amplitude of the $Al_{0.33}Ga_{0.67}As$/GaAs sample decreases only by 20%, while the phase difference varies by about 20 degrees for undoped AlGaAs, and 25 degrees for C-doped AlGaAs. Table 10 presents the results of the best fits of the model (formula 8) to the experimental data for undoped AlGaAs thin film. The other parameters appeared in formula (8) are given in Table 4.

Table 10. Thermal and infrared properties of the undoped $Al_{0.33}Ga_{0.67}As$ layer estimated using best fits of formula (8) to the normalized experimental data. Geometrical (thickness), thermal (thermal conductivity, diffusivity, thermal boundary resistance) and infrared (infrared absorption coefficient) are listed in Table 4 [H6].

Known parameters	Filter	Spectral range (nm)	Estimated Parameters		R^2
			k_1(W/mK)	α_1 x 10^{-6} (m^2/s)	
Infrared and geometrical parameters	F6	5585-6805	13.0 ± 2.0	5.8 ± 0.7	0.989
	F9	8900-9395	12.0 ± 1.0	5.9 ± 0.6	0.996
	F10	9650-11250	12.0 ± 1.0	6.0 ± 0.4	0.994
			$\beta_{I,R1}$ x 100 (m^{-1})		
Thermal and geometrical parameters	F6	5585-6805	0.0 ± 60.0		0.990
	F9	8900-9395	0.2 ± 25.0		0.993
	F10	9650-11250	0.3 ± 25.0		0.993

The obtained values of the thermal conductivity and diffusivity of the thin film agree well with the data available in literature (k_1= 11.7 (W/mK) and α_1 = 6.5 x 10^{-6} (m^2/s)) [24]. It is worth emphasizing that for all used filters the derived values lie within estimated errors. This demonstrates that the spectrally resolved measurements increases the reliability of the estimating thermal parameters. This in turns shows the advantage of the PTR method over other thermal wave methods. Finally, when the thermal parameters and thickness of the sample are known, one can estimate the infrared absorption coefficient of the thin layer. The obtained results suggest that the layer is undoped. From C-V measurements the doping concentration is 5(2) x 10^{14} cm^{-3}, indicating that the infrared absorption coefficient of the thin layer can be neglected. This is because in mid- and long wavelength infrared range, the infrared absorption coefficient is proportional to the carrier concentration. It has to be pointed out that large values of the estimation of errors indicates that the method has lower sensitivity for the IR transparent thin film samples as discussed in the theoretical section in H6 and H8 (see Fig. 5 in H8). In addition, a supplementary FTIR measurements were performed of the layer in the reflection configuration. Due to high infrared absorbing nature of the substrate, it is not possible to measure the sample in the transmission configuration. It was found that only reliable information which can be deduced is the layer thickness (see Fig. 6 in H6).

Since the doping of the sample only slightly lower values of thermal conductivity and diffusivity (see Table 4). Taking into account that both thin layers have almost the same thicknesses (see Table 4), the changes in the normalized signal are caused by only two parameters : the infrared absorption coefficient of thin layer and the thermal boundary resistance. Doping of the semiconductor causes increase of the infrared absorption coefficient. If so, taking into account the simulation presented in H8 (see Fig. 2 in H8), one should expect decrease of the phase difference. In fact, we didn't observe such effect. In turns, we observed the increases of the phase difference which suggests, based on a simulation presented in H8 (see Fig 3 in H8), that the thermal boundary resistance is relatively large. Table 11 presents

the results of the best fits of the theoretical model formula (8) to the experimental data for C-doped AlGaAs thin film obtained with k_1 = 10.8 W/mK and α_1=5.85x10^{-6} m^{2}s^{-1} (see Table 4).

Table 11. Thermal boundary resistance and infrared absorption coefficient of the C-doped $Al_{0.33}Ga_{0.67}As$ layer estimated using best fits of formula (8) to the normalized experimental data. The determination coefficient R^2 and the relative expanded uncertainties u_r are also given [H8].

Filter	Spectral range (nm)	Estimated Parameters				R^2
		R_{th} x 10^{-9} (m^{2}KW^{-1})	u_r	$\beta_{IR,1}$ (cm^{-1})	u_r	
F6	5585-6805	150 ± 25	0.17	420 ± 40	0.09	0.989
F9	7800-9395	180 ± 25	0.14	300 ± 40	0.13	0.991
F10	9650-11250	180 ± 25	0.14	210 ± 50	0.24	0.989

It is worth emphasizing that the thermal boundary resistance is constant within estimation errors for all used IR filters which, in addition, demonstrates that it is possible to estimate simultaneously these parameters. From Table 11 one can see that the thermal boundary resistance is almost two order of magnitude larger than for ideal thermal boundary resistance in AlGaAs/GaAs systems [H6]. This can be due to formation of the 2-dimensional hole gas due to the modulation doping [42]. As a result, phonons are scattered at the interface by the 2-dimensional hole gas [43], hence the thermal conductance of the interface is reduced. The disorder introduced by the impurities in the doped structure can also contribute to the thermal boundary resistance, however, this effect mainly decreases values of thermal transport parameters of thin film which is taken into account by setting lower values (compare to undoped structure) of thermal conductivity and diffusivity of thin film (see Table 4). Moreover, the contribution of interface roughness to thermal boundary resistance is very small, since the buffer layer is used to make atomically flat interfaces. In summary, the contributions of the interface roughness and the effect of disorder at the interface are very small compare to the contribution of the scattering of the phonons on 2-dimensional hole gas.

As one can see from Table 11 the infrared absorption coefficient of the thin layer decreases with increasing wavelength. It is worth mentioning that with increasing infrared absorption coefficient of the thin film, the sensitivity of the method for measuring $\beta_{IR,1}$ increases (Fig. 4 in H8) while the estimation error of $\beta_{IR,1}$ decreases (the relative expanded uncertainties in Table 12). It is expected that for the binary semiconductors for moderate doped material in mid infrared range the absorption is mainly caused by free carrier absorption. A characteristic feature of the free carrier absorption is that with increasing wavelength the infrared absorption coefficient also increases. Apart from the free carrier absorption for heavily doped materials, in p-type semiconductor also the absorption can be caused by the inter-valence band (IVB) absorption by holes. In fact the infrared spectra of p type doped GaAs (used as a substrate in this work) exhibit both contributions [H5]. One of the possible mechanisms of the IVB absorption is a transition between light to heavy holes. Infrared absorption coefficient describing this transition can be represented by the following simplified formula [44]

$$\beta_{IR}(\lambda) = a(N) \cdot \sqrt{\frac{1}{\lambda}}\left(e^{\left(-b\frac{1}{\lambda}\right)} - e^{\left(-c\frac{1}{\lambda}\right)}\right) \tag{24}$$

where *a*, *b* and *c* are constants and *N* is the carrier concertation. Figure 20 presents numerical simulation of the formula (24) and the estimated values of the infrared absorption coefficient in C doped $Al_{0.33}Ga_{0.67}As$.

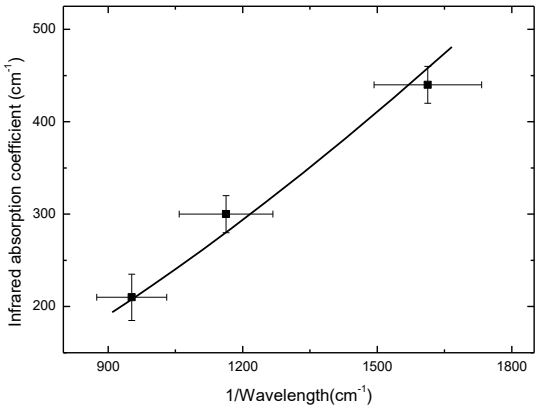

Fig. 20. Infrared absorption coefficient of C doped $Al_{0.33}Ga_{0.67}As$ thin film (point) as a function of inverse wavelength. The solid line is numerical simulation of the model described by formula 23.

As one can see from Fig. 20 the changes of the infrared absorption coefficient as a function of wavelength are well predicted by formula 24, this suggests that the absorption is caused by inter-valence band absorption by holes, as expected for p-type doped alloys(mixed) semiconductors. However, in contrast to binary semiconductors, the IVB absorption in alloy semiconductors is observed at shorter wavelengths and at lower hole concentrations. For example, the IVB absorption can dominate the infrared spectra in the mid-infrared range as it was observed in undoped $Ga_{0.32}In_{0.68}Sb$ bulk crystal [45]. While for thin films of Be doped $Al_{0.01}Ga_{0.99}As$ alloys the absorption was found to be due to free hole absorption [46]. This could be explained by the fact that $Al_{0.01}Ga_{0.99}As$ alloys have properties similar to those of binary GaAs as the mole fraction of aluminium is very small.

Table 12 presents summary of the integral and spectrally resolved PTR measurements.

Table 12. Comparison between spectrally integral and resolved PTR experiments of semiconductors.

Feature	Spectrally Integral PTR	Spectrally resolved PTR	Comments
Signal to noise ratio (SNR)	Optimal	Lower	SNR in SR-PTR depends on bandpass of IR filters, smaller bandpass leads to lower SNR; this can be avoided by higher power laser (~500 mW)
Measurement of a weak IR absorbing sample	Optimal	Possible	Depending on IR absorption coefficient one can get different SNR of thermal component in the PTR signal
Measurement of the thermal properties of the sample	Possible	Possible	In the case of the spectrally integrated measurements the use of an mean value of the infrared absorption coefficient should be tested
Reliability of estimation thermal parameters	Standard	improved	For each IR filters the same values of the thermal parameters of the sample are retrieved [H5,H6,H8]
Identification of physical processes in the sample	no possible	possible	Distinction between free carrier absorption and intervalence band transitions absorption in p-type GaAs possible only using SR-PTR method [H5]
Separation of the photothermal/photocarrier from photoluminescence components	no possible	possible	The separation of the components decreases the estimation errors of the parameters (ref. [H7])
Identification of measured lifetime using phenomenological model	no possible	possible	Please note that MgF_2 does not enough filter PT response, thus choosing of IR filter is crucial [H2, H7].
Infrared absorption or/and PL spectra	no possible	possible	Depending on the material properties, it is even possible to retrieve absorption and emission spectra using the same experimental set-up [H7]

As one can see from Table 12 the proposed methodology significantly improves the standard method like the PTR is and can be considered as an valuable extension of the optical metrology.

4.6. Imaging method of investigation thermal and infrared properties of semiconductors

The standard PTR method is one of the most widely used non-destructive techniques for characterizing various types of solids providing a local information at the position of the laser heating spot. For non-homogenous samples the main benefit of lock-in thermography (LIT) technique compared to PTR consists in the possibility of gathering information concerning the thermo-optical properties on a wide area of the sample. Although it is possible to obtain in-plane thermal properties of the sample using the PTR method, a simple modification of the LIT experimental set-up allow to measure in-plane thermal diffusivity (Fig. 1d). Due to technical limitation the measurements have to be performed in the transmission configuration (see light source in Fig 2 in H3). The expression for the PTR signal in the transmission configuration (assuming the one-dimensional approximation) can be written as follows [47]:

$$S\left(f,\beta_{eff,IR}\right)=\frac{T_{ap2}\beta_{eff,IR}}{2k\left(\beta_{eff,IR}^{2}-\sigma^{2}\right)}\left[\frac{2(g+t)-\left[(t+1)(1+g)e^{\sigma L}+(t-1)(1-g)e^{-\sigma L}\right]e^{-\beta_{eff,IR}L}}{(1+g)^{2}e^{\sigma L}-(1-g)^{2}e^{-\sigma L}}\right] \quad (25)$$

gdzie T_{ap2} is the instrumental factor and $g=k_0\sqrt{\alpha}/k\sqrt{\alpha_0}$, where index 0 refers to air.

The IR images are recorded by a thermographic camera equipped with a quantum detector array consisting of 256x320 infrared InSb detectors, 1pitch=15x15μm^2. Provided that the theoretical specifications are met the signal recorded by each pixel of the IR camera can be expressed by Eq. (25).

The resulting DC and phase images at f_0=25Hz are shown in Figure 21 (a, b). A rectangle S with a selected area of 18x21pixels (the corresponding area on image is S=6x7 mm^2, 1pixel≅0.33mm) was then subdivided into nine equal squares, each of them having an area of A_{sq}=6x7 pixels, as can be seen in Figure 18(b). The phase corresponding to each square was calculated as the average value of each pixel (located inside the square). For each excitation frequency, the subsequent phase images were computed and the same analysis procedure was applied. The model described by formula (24) were fitted, using the Matlab function *lsqcurvefit*, to the collected data points, after subtracting 180° from the corresponding experimental data.

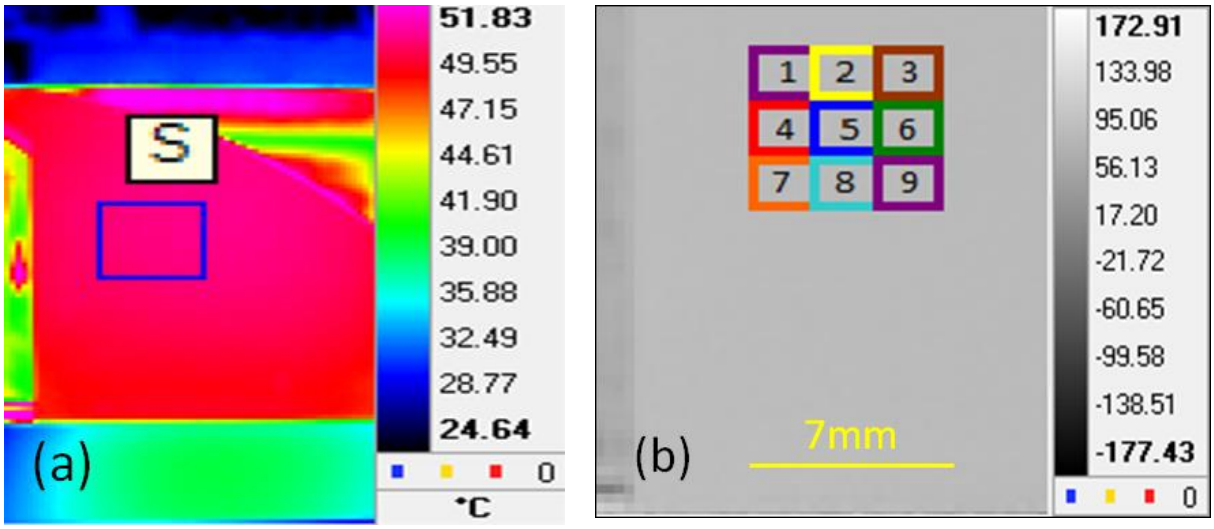

Figure 21. IR images of GaAs wafer: DC image (a) and the enlarged phase image (b) at 25 Hz.

For computations the thermal conductivities of the GaAs sample and air were set at 50 W/mK and k_g=0.026 W/(m·K), respectively, while the thermal diffusivity of air was set at $\alpha_g=31\cdot10^{-6}$ m^2/s. The best fits of the theoretical phases to the experimental data are shown in Figure 22.

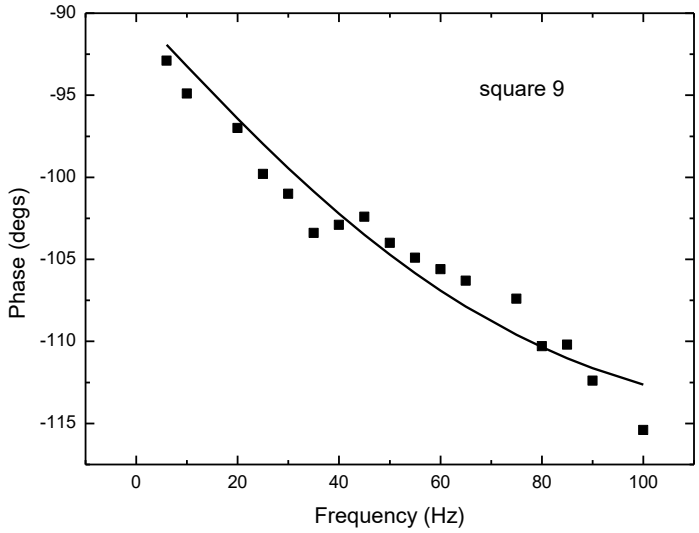

Figure 22. The best fits of the model formula (25) to experimental curve for square 9.

As one can see, the model predicts very well the experimental data for each square in figure 22. The resulting thermal diffusivities and effective infrared absorption coefficients obtained by using both LIT (from Fig. 23) and PTR methods are collected in Table 13.

Table 13. Effective infrared absorption coefficient and thermal diffusivities of n-GaAs wafer measured using LIT and PTR methods [H3, 13].

Method (detection range)	Thermal diffusivity (cm^2/s)	Effective infrared absorption coefficient (cm^{-1})
LIT (1.5-5.1μm)	(0.25÷0.27)±(0.03÷0.04)	26.60÷28.40
PTR (2-12 μm)	0.25±0.03	154.00

In order to demonstrate the uniqueness of the obtained solutions, the χ^2 test was performed and results are reported in H3. The accuracy of the estimating parameters could probably be improved by using a homogeneous laser beam spread on the sample surface. The resulting thermal and optical parameters, together with corresponding errors (≅10%), are gathered in Table 13. The errors are calculated using the Matlab function nlparci which returns the 95% confidence intervals for the nonlinear least squares parameters in nonlinear model. The model described by formula (24) can be applied directly to each pixel in the phase images. Figure 23 shows the thermal diffusivity and effective infrared absorption images, respectively, obtained from the raw phase values (a and b).

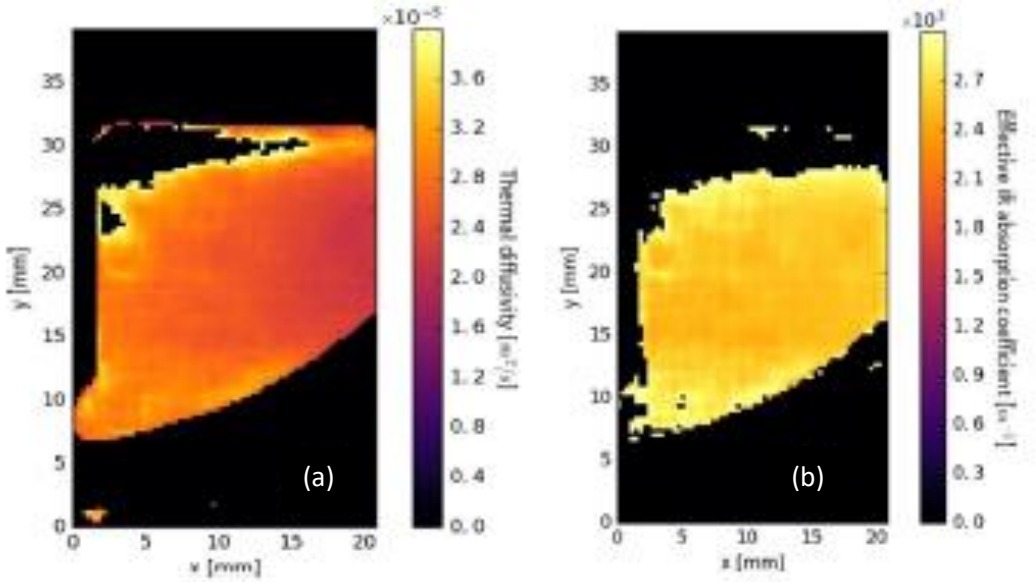

Figure 23. Thermal diffusivity and effective infrared absorption coefficient images of GaAs wafer: (a) thermal diffusivity and (b) effective infrared absorption coefficient values obtained directly from the fitting of raw phase values and next improved using a median filter (7x7 pixels) [13].

Table 14 presents the comparison between modulated photothermal infrared radiometry and lock-in thermography methods.

Table 14. Comparison between the lock-thermography and modulated photothermal infrared radiometry techniques [13].

Feature	Modulated photothermal infrared radiometry	Lock-in thermography
Area of investigation	Local, Large area possible using PTR microscopy, however the analysis is complicated (see Resolution)	Large
Time required to collect image	Long	Short
Resolution	Depending on the laser beam size (lateral heat as in Fig. 1), however several hundreds of micrometers is possible	Depending on the resolution of the IR camera lens;
Modulation frequency (the higher frequency the thinner film can be investigated)	High, up to 20 MHz	Medium (several hundred Hz)
Costs	Relatively low	Very High

As one can see, the lock-in thermography technique is more appropriate than modulated photothermal infrared radiometry technique for the investigation of large area of bulk semiconductor materials, whereas the modulated photothermal infrared radiometry method is more suited for the investigation of thinner films

5. Summary

In the last decade the photothermal IR radiometry (PTR) method has found wide applications in the field of non-destructive evaluation of materials. A weak point of the conventional approach, however, is the disregard of the influence of the IR properties of the sample on the IR signal. The main achievement of the proposed series of publications is the introduction of a new IR-spectroscopic approach based on the spectrally resolved PTR (SR-PTR) that uses the thermal and plasma wave formalisms. Besides a more precise determination of the thermal and electronic parameters the new concept offers a new IR-spectroscopic tool for special samples which are not or only hardly accessible to the conventional IR-spectroscopic techniques.

In particular with the series of publication discussed in this report the following progress and improvements could be achieved with regard to the investigation of the IR-properties of a sample using the PTR method:

1. Development of three different methods based on PTR for the estimation of the infrared absorption coefficient of bulk samples. An important aspect for the application is that only measurements in one (reflection) configuration are necessary [H1,H5,H9];
2. Evidence that the precision of estimation of the thermal diffusivity of the bulk samples depends on the infrared properties of the samples. Very high precision of estimation of the thermal diffusivity can be achieved for highly IR absorbing samples [H4]; The precision of estimation of the infrared absorption coefficient of bulk samples is independent of the magnitude of the infrared absorption coefficient.
3. Proof that SR-PTR method is able to measure the infrared absorption coefficient of highly IR absorbing samples [H5];
4. Demonstration that SR-PTR method is able to measure thermal and infrared properties of the thin films. The method is particularly effective for the investigation of thin films deposited on highly IR absorbing substrate [H6,H8]; The precision of estimation the infrared absorption coefficient increases with increasing infrared absorption coefficient,
5. Development of a method to retrieve maps of thermal (thermal diffusivity) and infrared properties of the bulk samples using lock-in thermography [H3];
6. Demonstration that the SR-PTR can be used to uncover photoluminescence components enabling to retrieve absorption and photoluminescence spectra of the sample using one experimental set-up [H1, H2, H2a,H7];
7. Proof that the SR-PTR method allows very accurate measurement of the recombination lifetimes like in ZnSe:Cr crystals. [H7];
8. Use of the SR-PTR method to control the IR band gap required in order to take into account correctly the infrared property for the estimation of the thermal and electronic parameters of a semiconductor sample [H9].

Finally the advantages and disadvantages of the SR-PTR method as compared to the established FTIR spectroscopic methods for the investigation of solid samples are listed in Table 15.

Table 15. Comparison between SR-PTR and FTIR methods.

	FTIR	FTIR-PAS	SR-PTR
Sample size	Limited by the dimension of the apparatus	Limited by the photoacoustic chamber	No limit
Sample preparation	Ambitious	Simple	Simple
Highly IR absorption thick sample	Not possible	No information available	Possible
Spatial (depth) resolution	No	Poor because modulation frequency < 1 kHz	High because modulation frequency up to 20 MHz possible,
Spectral resolution	High	High	Very low
Simultaneous absorption and PL spectra	No	No	Possible
Time required to collect spectra	Short	Short	Long
Estimation of the infrared absorption coefficient β_{IR}	Possible, but measurements in transmission and reflection configuration are required (or the reflectivity) must be assumed	Not possible	Possible, when thermal parameters are known then β_{IR} of the substrate and thin film can be simultaneously estimated
Other information	No	Thermal properties or thickness	Recombination lifetime or/and thermal properties or thickness
Costs	High	High	Relatively low
Possible industrial application	Difficult	Difficult	Simple, see example apparatus in [46]

Although the spectral resolution of the SP-PTR is lower than that of the conventional methods it is sufficient for the investigation of semiconductor samples which exhibit broad absorption bands. The spectral resolution of the SP-PTR achieved in the reported studies (measurements were performed using 150 mW diode laser except for H1) could be increased significantly if a higher laser power is used . As one can see from table 14, the SR-PTR method combines also features of the calorimetric and conventional PL methods, and should be considered as supplementary to other methods. A unique feature of the SR-PTR method is that it can be used for remote studies e.g. in industrial plants or in basic research to estimate doping levels of thin films (after a calibration to Hall measurement performed on thin films grown on undoped sample) where the electrical methods fail. With Hall measurement one can not measure the concentration in doped and undoped thin films due to influence of heavily doped substrate [H6,H8], while with the C-V spectroscopy one is not able to measure the concentration in doped thin film [H8]. Finally, the proposed thermal wave method can be also used to study spatial variation of the physical properties of doped semiconductor samples like infrared (infrared absorption coefficient is proportional to the doping concentration) and

thermal (thermal diffusivity) parameters using the lock-in thermography (as it was demonstrated in H3 for moderate doped GaAs sample) that delivers infrared (also spectrally resolved) and thermal diffusivity images.

It is worth to emphasise that the knowledge of the IR absorption coefficient is necessary to retrieve correct values of the thermal and electronic parameters of the non IR opaque samples. The infrared absorption coefficient has a large impact on the depth dependence of the measured parameters retrieved from their variation with modulation frequency since with the increasing infrared absorption coefficient the PTR arise closer to the surface. Moreover, the knowledge of the infrared absorption coefficient can also increase the accuracy of estimation carrier recombination parameters especially for moderately doped samples.

It is planned to focus the future works on the investigation of thermal and infrared properties of III-V superlattices, thin organic films and II-VI bulk semiconductor samples. In order to accomplish these projects a new experimental set up is constructed that uses a high power laser 532 nm DPSS laser (~1 W) to improve the SNR and extended modulation frequency range up to 10 MHz increasing the spatial resolution. The main new feature of the set-up is a sample cell for temperature dependent PTR measurements in the range from -196 °C to 420 °C.

Finally it has to be pointed out that the method can be easily adopted in industry. Fig. 24 presents the optical block of the PTR system constructed with cooperation of the author of the proposal with prof. Mandelis group.

Fig. 24 Optical block of the PTR device used in Avio. Detailed information of the devices can be found in Ref.48.

It is worth to emphasize that the IR detector used in the device is produced by the Polish company Vigo. Using presented apparatus in Fig. 24 it is possible to measure carrier concentration in semiconductor materials. For example, in order to calculate carrier concentration one can use the following formula [49]

$$n = \frac{\beta_{IR}}{7.5 \cdot \lambda^3} 10^{20} \ (cm^{-3}), \tag{26}$$

where λ is wavelength in μm and β_{IR} is the infrared absorption coefficient at λ in cm^{-1}. This formula is valid for n type GaAs which have carrier concentration between 10^{17} and 10^{18} cm^{-3}.

Assuming (very inaccurate assumption) that the effective infrared absorption coefficient is measured for wavelength 11.3 μm, which is wavelength for the maximum sensitivity of the

detector, one can estimate the carrier in n-GaAs (S6) using formula (18) to $(1.42 \pm 0.14)x10^{18}$ cm^{-3}. Supplementary Hall measurements yield the value $1.7x10^{18}$ cm^{-3}, which is in a good agreement with this measured using the PTR method. The accuracy of the PTR method can be easily improved by applying the SR-PTR method.

References

[1] P. E. Nordal and S. Kanstad, "Photothermal radiometry," Phys. Scr. 20, 659–662 (1979).

[2]] N. Horny, M. Chirtoc, A. Fleming, G. Hamaoui, and H. Ban, Kapitza thermal resistance studied by high-frequency photothermal radiometry, Appl. Phys. Lett. **109**, 033103 (2016).

[3] M. Pawlak, M.Maliński, Noncontact measurement of the thermal diffusivity of IR semi-transparent and semiconducting n-CdMgSe mixed crystals by means of the photothermal radiometry, Infrared Phys Techn 64 (2014), 87-90

[4] U. Seidel, and H. G. Walther, The influence of the spectral emissivity on the signal phase at photothermal radiometry, Review of Scientific Instruments 67, 3658 (1996);

[5] B. Majaron, M. Milanic, Effective infrared absorption coefficient for photothermal radiometric measurements in biological tissues, Phys. Med. Biol. 53 (2008) 255–268

[6] M. Nestoros, A. Gutierrez-Llorente, A. Othonos, C. Christofides and J. M. Martinez-Duart, "Photothermal radiometric and spectroscopic measurements on silicon nitride thin films", J. Appl. Phys. 82, 6215-6219 (1997).

[7] S. Paoloni, and H. G. Walther, Photothermal radiometry of infrared translucent materials, Journal of Applied Physics 82, 101 (1997);

[8] A. Mandelis, A.Othonos, C.Christofides, J.Boussey-Said, Non-contacting measurements of photocarrier lifetimes in bulk- and polycrystalline thin-film Si photoconductive devices by photothermal radiometry J. Appl. Phys. 80 5332 – 5341 (1996)

[9] D. Shaughnessy , A. Mandelis, Carrier-density-wave transport property depth profilometry using spectroscopic photothermal radiometry of silicon wafers I: Theoretical aspects J. Appl. Phys. 93, 5236-5243 (2003)

[10] D. Shaughnessy, A. Mandelis, Carrier-density-wave transport property depth profilometry using spectroscopic photothermal radiometry of silicon wafers II: Experimental and computational aspects, J. Appl. Phys. 93, 5244-5250 (2003)

[11] A. Salnick, C. Jean and A. Mandelis, Noncontacting Photothermal Radiometry of SiO2/Si MOS Capacitor Structures, Solid State Electron 41 (4), 591-597 (1997)

[12] B. Li S.Zhang, The effect of interface resistances on thermal wave propagation in multi-layered samples, J. Phys. D: Appl. Phys. 30 (1997) 1447

[13] M. Pawlak. K. Ramza, M. Streza, Simultaneously Mapping of In-Depth Thermal Diffusivity and Effective Infrared Absorption Coefficient of Silicon-Doped Gallium Arsenide Wafer Using Lock-in Thermography, Anal. Letters. **52** (2019) 93-101

[14] R.Fuente, E,Apinaniz, A.Mendioroz, and A. Salazar, Simultaneous measurement of thermal diffusivity and optical absorption coefficient using photothermal radiometry. I. Homogeneous solids, Journal Of Applied Physics 110, 033515 (2011)

[15] M. Chirtoc, Chap. 2, in: "Thermal Wave Physicsand Related Photothermal Techniques", E. Marín Moares (Ed.), Transworld Research Network, Trivandrum, Kerala, 2009 (trnres.com).

[16] M. Pawlak, Thermal and plasma waves in semiconductor, PhD Thesis, Koszalin, 2014

[17] A. Salnick, A. Mandelis, H. Ruda, C. Jean, Relative Sensitivity of Photomodulated Reflectance and Photothermal Infrared Radiometry to Thermal and Carrier Plasma Waves in Semiconductors, J. Appl. Phys. 82, No. 4, 1853-1859 (1997)

[18] T. E. Milner, D. M. Goodman, B. S. Tanenbaum and J. S. Nelson, Depth profiling of laser-heated chromophores in biological tissues by pulsed photothermal radiometry, J. Opt. Soc. Am. A 12 1479–88 (1995)

[19] M. Pawlak, S. Pal, S.Scholz, A.Ludwig, A.D.Wieck,

[20] M. Reichling, H. Groenbecka, Harmonic heat flow in isotropic layered systems and its use for thin film thermal conductivity measurements, J. Appl. Phys., 75 (4) (1914), p. 1994

[21] S.J. Sheard, Non-contacting determination of carrier lifetime and surface recombination velocity using photothermal radiometry, Materials Science and Engineering: B Vol. 5, Issue 2, January 1990, 101–105

[22] J. Tolev, A. Mandelis, M. PawlakNon-linear dependence of photocarrier radiometry signals from p-Si wafers on optical excitation intensity, J. Electrochem. Soc., 154 (11) (2007), pp. H983-H994

[23] R.D. E.Aspnes, S.M. Kelso, R.A. Logan, R. BhatOptical properties of AlxGa1-xAs,J. Appl. Phys., 60 (1986), p. 754

[24] S. AdachiAlAs GaAs, and AlxGa1-xAs. Material parameters for use in research and device applications, J. Appl. Phys., 58 (1985), p. R1

[25] M.S. Vitiello, G. Scamarcio, V. Spagnolo, Temperature dependence of thermal conductivity and boundary resistance in THz quantum cascade lasers, IEEE J. Sel. Topics Quantum Electron., 14 (2008), pp. 431-435

[26] M.E. Rodriguez, A. Mandelis, G. Pan, L. Nicolaides, J. Garcia, Y. Riopel, Computational aspects of laser radiometric multiparameter fit for carrier transport property measurements in Si wafers, J. Electrochem. Soc., 147 (2) (2000), pp. 687-698

[27] M. Soltanolkotabi, G.L. Bennis, R. Gupta, Temperature dependence of the thermal diffusivity of GaAs in the 100-305 K range measured by the pulsed photothermal displacement technique, J. Appl. Phys., 85 (1999), p. 794

[28] M. Pawlak, F. Firszt, S. Łęgowski, H. Męczyńska, Gibkes, Pelzl, Thermal Transport Properties of Cd1-xMgxSe Mixed Crystals Measured by Means of the Photopyroelectric Method, Int. J. Thermophys. 31 (2010), 187-198

[29] G. Amato, G. Benedett, R. Spagnol, M. TurnaturPhotoacoustic measurements of doped silicon wafers, Phys. Status Solidi A, 114 (2) (1989), pp. 519-523

[30] R.O. Carlson, G.A. Slack, S.J. Silverman, Thermal conductivity of GaAs and GaAs1-xPx laser semiconductors, J. Appl. Phys., 36 (2) (1965), p. 505

[31] M. Pawlak, S. Pal, A.Ludwig, A.D.Wieck, Journal of Applied Physics 122, 229901 (2017)

[32] M. Pawlak, M.Maliński, F. Firszt, S. Łęgowski, H. Męczyńska, J.Ollesch, A.Ludwig, A.Marasek, C. Schaulte-Braucks, Investigation of carrier scattering mechanisms in n-Cd1-xMgxSe single crystals using Fourier Transform Infrared Spectroscopy, Infrared Phys. Techn. **64** (2014), 115-118

[33] A. Adachi, Optical constants of crystalline and amorphous semiconductors: numerical data and graphical information,Kluwer Academic, Boston (1999)

[34] P.K. BasuTheory of optical processes in semiconductors, Oxford Clarendon Press (1997)

[35] K. Perzyńska, F. Firszt, S. Łęgowski, H. Męczyńska, J. Szatkowski,, M. Biernacki, A. Gajlewicz, S. Tarasenko, P. Zaleski, Hall effect investigations of Cd1-xMgxSe bulk crystals, J. Cryst. Growth 214/215 (2000), 904-908

[36] M. L. Huberman, A. Ksendov, A. Larsson, R. Terhune, and J. Maserjian, Phys. Rev. B 44 1128 (1991).

[37] Y. Lao, and A. G. Unil Perera, J. Appl. Phys. 109 103528 (2011).

[38] S. B. Mirov, V. V. Fedorov, D.Martyshkin, I.S. Moskalev, M. Mirov, and S. Vasilyev, IEEE Journal of Selected Topics in Quantum Electronics 21 (2015)

[39] J. Peppers, V. V. Fedorov, and S. B. Mirov, Optics Express 423 (2015) 4470

[40] M. Luo, B. L. Van Mil, R. P. Tompkins, T. H. Myers, and N. C. Giles, J. of Appl. Phys. 97 (2005) 013518

[41] J.Wang, A.Mandelis, A. Melnikov, S. Hoogland, and E. H. Sargent, J. Phys. Chem. C 117 (2013) 23333

[42] L. L. Chang, K. Ploog, Molecular Beam Epitaxy and Heterostructures, Martinus Nijhoff Publishers (1985)

[43] S. Adachi, Properties of Aluminium Gallium Arsenide, The Institution of Engineering and Technology, 1993 ,p. 183

[44] A. H. Kahn, Theory of the Infrared Absorption of Carriers in Germanium and Silicon, Phys. Rev. 97, 1647 (1955).

[45] A. Chandola, H. J. Kim, P. S. Duttaa, S. Guha, L. Gonzalez, V. Kumar, Below band-gap optical absorption in GaxIn1−xSb alloys, J. Of Appl. Phys. 98, 093103 2005

[46] M. B. M. Rinzan, D. G. Esaev, A. G. U. Perera, S. G. Matsik, G. Von Winckel, A. Stintz, and S. Krishna, Free carrier absorption in Be-doped epitaxial AlGaAs thin films, Appl. Phys. Lett. 85, 22 (2004).

[47] A. Mandelis, Diffusion-Wave Fields, Springer Verlag, New York, 108 (2001) p.109.

[48] X. Guo, K. Sivagurunathan, M. Pawlak, J. Garcia, A. Mandelis, S. Giunta, S. Milletari,S. Bawa, Laser Photothermal Radiometric Instrument For Industrial Steel Hardness Inspection, J. Phys. Conf. Ser. **214** (2010)

[49] http://www.ioffe.ru/SVA/NSM/Semicond/GaAs/optic.html

6. Discussion of the other scientific (artistic) accomplishments.

Between 2001 and 2004 I have worked (at the beginning of student assistant and later as PhD candidate) as a researcher at the Department of Semiconductor and Carbon Physics of Institute of Physics NCU dealing with preparation and study of thermal and optical properties of broadband ternary and quaternary II-VI compounds using photothermal piezoelectric technique. In 2004 I have received a position at the Institute of Experimental Physics III (prof. Pelzl group) as a scholarship holder in the frame of the GRK 384: Nanoelektronische, mikromechanische und mikrooptische Systeme: Analyse und Synthese mittels Ionen, Elektronen und Photonen. Doctoral thesis entitled "Thermal and electrical properties of semiconductors measured by means of photopyroelectric and photocarrier radiometry techniques" I have defended and got a PhD in physical sciences (dr rer. nat. doctor rerum naturalium) 10th January 2010. One of the achievement of the doctoral thesis was a development of the photocarrier radiometry (PCR) method. The work was performed in co-operation with prof. Mandelis from the University of Toronto. Laser infrared photocarrier radiometry (PCR) is based on a harmonically modulated low-power laser pump and a superposed dc superband-gap optical bias (a secondary laser beam)to control and monitor the space-charge-layer (SCL) width in oxidized pSi–SiO_2 and nSi–SiO_2 interfaces (wafers) exhibiting charged interface-state related band bending. Applying the theory of PCR-SCL dynamics to the experiments yielded various transport parameters of the samples as well as depth profiles of the SCL exhibiting complete (p-type Si) or partial (n-type Si) band flattening, to a degree controlled by widely different minority-carrier capture cross section at each interface [1]. It was found that the conventional linear approach is not always consistent with experimental slopes of amplitude vs power and it may yield erroneous values of the electronic transport properties [2]. It was shown that the amplitude of the PCR signal exhibits a supralinear dependence on laser intensity I_0^{β} , with nonlinearity coefficient/exponent β such that $1 \leq \beta \leq 2$. The power dependence of the amplitude is an important indicator of the photo-excited carrier recombination physics in semiconductors ranging between monopolar $(\beta=1)$ and bipolar $(\beta=2)$ limits. Moreover, the thermal properties of CdMgSe was studied on the self-constructed photopyroelectric (PPE) set up in the temperature range between 20ºC and 40ºC [3]. In the meantime at the University of Toronto in prof. Mandelis group [4] I also participated in the construction of the one of the first PTR apparatus which was used in industry (Avio, Italy).

Between 04.2009 and 01.2012 I had to work outside science and I decided to continue my scientific carrier as a PhD student in prof. Maliński´s group at Technical University of Koszalin (instead of nostrification of the received PhD in Germany). Since 02.2012 I have received an adjunct position at Institute of Physics NCU. Doctoral thesis entitled "Thermal and plasma waves in semiconductors I have defended and got a PhD in technical sciences 18th July 2014. In the frame of this thesis the thermal and recombination of CdMgSe crystals and ion implanted silicon samples were investigated [5-7]. Particularly the effect of the thin IR opaque layer on the estimation of the thermal diffusivity of CdMgSe crystals investigated in the transmission configuration was investigated. It was found that the information about the thermal and geometrical parameters of the opaque layer should be known. The simplified model of the PTR signal in order to estimate recombination was also proposed [6,7]. After receiving PhD degree I started investigated the effect of the infrared properties of the sample

on the PTR signal in the transmission configuration [8]. The effect of the signal interference in the sample on the overall PTR signal and estimation of the thermal diffusivity and absorption coefficient was discussed [9]. It was found that the this effect cannot be neglected in relatively thin samples (usually less than 1 mm). In addition a physical interpretation of the reduction of the PTR amplitude with decreasing wavelength of a laser beam for ion implanted samples were given [10-11]. It turns out that the reduction is caused by increasing of the optical absorption of the implanted layer.

Literature

[1] A. Mandelis, J. Batista, J. Gibkes, M. Pawlak, J. Pelzl, Noncontacting laser photocarrier radiometric depth profilometry of harmonically modulated band bending in the space-charge layer at doped SiO2-Si interfaces,J. Appl. Phys. 97 (2005), 083507

[2] J. Tolev, A. Mandelis, M. Pawlak, Nonlinear dependence of photocarrier radiometry signals from p-Si wafers on optical excitation intensity, J. Electrochem. Soc. 154 (11) (2007), H983-H994

[3] M. Pawlak, F. Firszt, S. Łęgowski, H. Męczyńska, Gibkes, Pelzl, Thermal Transport Properties of Cd1-xMgxSe Mixed Crystals Measured by Means of the Photopyroelectric Method, Int. J. Thermophys. 31 (2010), 187-198

[4] X. Guo, K. Sivagurunathan, M. Pawlak, J. Garcia, A. Mandelis, S. Giunta, S. Milletari,S. Bawa, Laser Photothermal Radiometric Instrument For Industrial Steel Hardness Inspection, J. Phys. Conf. Ser. **214** (2010)

[5] M. Pawlak, M.Maliński, Noncontact measurement of the thermal diffusivity of IR semi-transparent and semiconducting n-CdMgSe mixed crystals by means of the photothermal radiometry, Infrared Phys Techn 64 (2014), 87-90

[6] M. Pawlak, M.Maliński,Minority carrier recombination lifetimes in n-type CdMgSe mixed crystals measured by means of the photothermal infrared radiometry Opto-Electron. Rev. 22 (1) (2014), 31-35

[7] M. Pawlak, M.Maliński, Influence of the Ar8+ and O6+ ion implantation on the recombination parameters of p and n type implanted Si samples investigated by means of the photothermal infrared radiometry, Infrared Phys Techn 63 (2014), 6-9

[8] M. Pawlak, M.Maliński, F. Firszt, J.Pelzl, A.Ludwig, A. Marasek, Linear relationship between the Hall carrier concentration and the effective absorption coefficient measured by means of the photothermal radiometry in IR semi-transparent n-type CdMgSe mixed crystals, Meas. Sci. Technol. 25 (2014), 035204-(8pp)

[9] M. Pawlak, Determination of the carrier concentration in CdSe crystals from the effective infrared absorption coefficient measured by means of the photothermal infrared radiometry, Appl. Phys. A 118 (2015), 173-176

[10] M. Pawlak, M.Maliński, Simultaneous measurement of thermal diffusivity and effective infrared absorption coefficient in IR semitransparent and semiconducting n-CdMgSe crystals using photothermal radiometry, Thermochim Acta 599 (2015), 23-26

[11] M.Maliński, M. Pawlak, Ł.Chrobak, S.Pal, A.Ludwig, Monitoring of Amorfization of the Oxygen Implanted Layers in Silicon Wafers Using Photothermal Radiometry and Modulated Free Carrier Absorption Methods, Appl. Phys. A 118 (3) (2015), 1009-1014

[12] Ł.Chrobak, M.Maliński, M. Pawlak, Measurements Of The Optical Absorption Coefficient Of Ar+8 Ion Implanted Silicon Layers Using The Photothermal Radiometry And The Modulated Free Carrier Absorption Methods, Infrared Phys Techn 67 (2014), 604-608

Invitation to write a Perspective for Journal of Applied Physics 24 Styczeń 2019 (Czwartek), 20:47

Od: "Andre Anders" <aanders@aip.org>

Do: "mispawlak@yahoo.pl" <mispawlak@yahoo.pl>

DW: "Andre Anders" <aanders@aip.org> "JAP Journal Manager" <jap-journalmanager@aip.org>

"mandelis" <mandelis@mie.utoronto.ca>

Liczba plików: 1 212kB

PDF 212kB

JAP Invited Perspectiv

Zapisz

January 24, 2019

Nicolaus Copernicus University
Jurija Gagarina 11
87-100 Torun
Poland

Dear Dr. Pawlak,

I am contacting you in my role as Editor-in-Chief of *Journal of Applied Physics* to invite you to write a Perspective article for the journal.

Since 2016, Perspectives have been a regular, highly cited, and highly downloaded feature of the journal. The Editors commission recognized experts in the field to write these articles on focused topics of current interest in applied physics research. Perspectives discuss recent advances in subfields of applied physics and where the research is headed. The authors present their personal views and opinions of developments that could lead to disruptive technologies, open questions, and possible solutions.

Perspective articles are made freely available to all for download for one year after publication without any charge to you, the author. Moreover, they are prominently highlighted on *Journal of Applied Physics'* website and benefit from AIP Publishing's marketing program. More detailed instructions and guidelines on how to write a Perspective for *Journal of Applied Physics* are provided in the attached document.

Following up on the recommendation by Associate Editor Andreas Mandelis, it is my pleasure to invite you to write a *Perspective* on the topic "Photothermal and photocarrier phenomena in semiconductors" (you may adjust the title to your liking). You are welcome to collaborate with coauthors on this paper. We would like you to submit your *Perspective* within **3-6 months** of receiving this invitation, but are flexible if this does not fit with your current schedule. The manuscript will be refereed, and, of course, the reviewers will be informed that it is an *Invited Perspective* article that must meet different expectations than a standard original research paper.

Please let us know if you accept my invitation by replying to aanders@aip.org and jap-journalmanager@aip.org. Please provide a tentative submission date and title by **February 7, 2019**. A list of coauthors and a brief synopsis of the article would also be welcome for our records. Our editorial office will periodically follow up with you as you prepare your manuscript for submission. If you have any questions, you can contact me or Dr. Benedetta Camarota, *Journal of Applied Physics'* Journal Manager, at the above email addresses.

I look forward to hearing from you. I hope you will contribute to *Journal of Applied Physics* through this important initiative for the applied physics community.

With best regards,

Andre Anders, Editor-in-Chief, *Journal of Applied Physics*